The Institute of Space and Astronautical Science
Report No. 637, September 1989

10 m Prototype for the Laser Interferometer Gravitational Wave Antenna

By

S. KAWAMURA, J. MIZUNO, J. HIRAO, N. KAWASHIMA, R. SCHILLING*

(January 25, 1989)

Summary: The 10 m prototype for the laser interferometer gravitational wave antenna was operated for an extended period to obtain information about the long-term operational stability and noise distribution. Stability of operation and noise statistics are particularly important for a future larger interferometer antenna. The prototype consists of an illuminating frequency stabilized Ar^+ laser, two perpendicular arms of 10 m in length, suspended mirrors acting as test masses, forming optical delay lines with a total path length of 1 km. Various kinds of noise sources were identified and successfully eliminated. Among them, laser frequency noise was suppressed below the current shot noise level by stabilizing the laser frequency by approximately 70 dB at a frequency of 1 kHz using rf-reflection-locking technique. As a result, the fundamental limit of shot noise corresponding to a light power of 30 mW was almost achieved above 3 kHz. The resultant sensitivity was $1.6\times10^{-18}/\sqrt{\text{Hz}}$ at 2 kHz and the noise floor above 6 kHz was $9.5\times10^{-19}/\sqrt{\text{Hz}}$ for the gravitational wave amplitude h. The system was continually operated for more than 100 hours over a period of 21 days and important new information was obtained. The data acquisition system worked without any trouble. Laser mode jumps, that may cause the breakdown of the system, were avoided carefully, while the instability of the laser mode turned out to be the major cause for the unlocking of the frequency stabilization system. No obstacles for the long-term operation were found in the main feedback control, except for a minor deterioration of the sensitivity with the passage of time. The optimal design of the feedback control system permitted the continuous operation of the 10 m prototype for more than 5 hours, whereas the longest continuous run of laser interferometer antennas ever done had been only 1–2 hours. The noise distribution of the interferometer output at low frequency suggested that the up-conversion noise of the scattered light is dominant around 1.5 kHz. Unidentified burst-like signals were found to exist even around 4 kHz where the effect of the up-conversion noise is low. Only 5 such bursts were detected in three hours of operation; this is infrequent enough to be easily eliminated by correlating the output of two antennas operating simultaneously.

* On leave of absence from Max-Planck-Institut für Quantenoptik, Garching, West Germany.

1. Introduction

The existence of gravitational waves was predicted as a consequence of the general theory of relativity by Einstein in 1918. Using a weak-field approximation, he formulated the gravitational wave, which travels at the speed of light, and demonstrated that systems with changing mass quadrupole moment can emit gravitational waves.

Although there is a very strong consensus among present-day physicists that gravitational waves do exist, no direct detection of gravitational waves has ever been accomplished. This is because of the very weak interaction of gravitational waves with matter.

To see the faintness of the interaction, the amount of radiation generated using a man-made device can be estimated as follows. A rod (mass M, length $2l$) rotating with an angular velocity ω about an axis perpendicular to the rod axis will generate gravitational waves. Its total power P_{GW} can be calculated using the general relativity:

$$P_{GW} = \frac{128\, GM^2 l^4 \omega^6}{45c^5},$$

where G is the gravitational constant and c is the velocity of light. For optimistic values of $M \simeq 10^7$ kg, $l=1$ m, and $\omega=10^3$, the power of the gravitational wave is

$$P_{GW} \simeq 10^{-20} \text{ W}.$$

This value can be converted to a strain in space due to the gravitational wave in the wave zone of the generator, at a distance of at least one wavelength of the gravitational wave (in this case, 2×10^6m). The resulting strain h is

$$h \simeq 10^{-37}.$$

Because of this discouragingly small value, laboratory generation of gravitational waves of detectable strength is unattainable.

Fortunately some astronomical sources have a considerably larger estimated value for the amplitude of gravitational waves at the earth, as compared with the man-made source. For example theoreticians predict that supernovas in the center of our galaxy will emit gravitational waves with a strain of 10^{-18} at the earth. Thus the most likely measurable gravitational waves, at present, would come from astronomical sources.

Indirect evidence for the existence of gravitational waves has been provided by the observation on the binary pulsar PSR 1913+16 [*1*]. The orbit of the binary pulsar is decaying at exactly the same rate expected because of gravitational-wave damping. The observed rate of orbital period change is $(2.40\pm0.09)\times10^{-12}$ s/s and the general relativity predicts $(2.403\pm0.002)\times10^{-12}$ [2]. This agreement has provided a most impressive, but indirect, evidence for the existence of gravitational waves. Still, one cannot completely rule out the unlikely possibility that tidal or mass-exchange effects, by chance, compensate for the rate predicted by the general relativity.

The direct detection of gravitational waves is undoubtedly one of the most challenging unsolved problems in experimental physics today. Success in this field would provide an important test, in a new regime, of the general relativity. Alternative theories of gravity usually also predict gravitational waves but with significant differences from the predictions of general relativity. In some theories the speed of gravitational waves may differ from that of light and in others, polarization properties may also differ.

The observation of gravitational waves might also open a new astronomical window. The gravitational-wave astronomy will provide a direct evidence for the physical properties and dynamics of the core of compact stars such as black holes and neutron stars, and also violent interactions such as supernovas, colliding neutron stars or black holes and coalescing binary systems.

Furthermore the detection of low-frequency gravitational waves might provide new insights about early stages of the big bang; the gravitational wave from an early inflationary era of the expanding universe is predicted to exist in the frequency range of millihertz and microhertz. There may also exist gravitational waves emitted from decaying cosmic strings, which would have been created by phase transitions in the early universe.

Experimental research for detecting gravitational waves is now under way in many laboratories around the world. Although gravitational waves have not yet been discovered, great advances in technology together with the strength of the current theoretical prediction lead one to expect that gravitational waves may be detected within the next decade.

In the early stages of research, J. Weber at the University of Maryland reported coincident excitation in two separate antennas [*3*]. The antennas used were high-Q resonant aluminium bars at room temperature with the resonant frequency tuned to 1.6 kHz. He attributed the excitation to gravitational-wave pulses emitted from a certain source in our galaxy. This, what is called the Weber event, stimulated a large number of other experimental searches for gravitational waves. Although none of the next series of experimental searches have produced positive results and there is much criticism on Weber's interpretation of data, this event must be considered as the first-phase in the progress of the development of gravitational wave antennas.

Current work on bar detectors is a continuation of the work started by Weber. Low temperature techniques to reduce thermal noise in aluminium bars up to 6 tons in mass are being implemented at a number of places. Among them the antenna in Stanford has achieved the best strain sensitivity of 10^{-18} for millisecond pulses [*4*]. Whereas most bar detectors aim at gravitational-wave bursts, Hirakawa, Tsubono and Fujimoto (University of Tokyo) have constructed a mechanical resonant detector at the frequency 60.2 Hz expected for radiation from Crab pulsar [*5*].

Two types of space-based experiments for detecting gravitational waves have also been achieved. One is Doppler tracking of interplanetary spacecraft and the other is pulsar timing. In either case, passing gravitational waves cause deviations in the distance between spacecraft or pulsars and the earth. Thus, gravitational waves can be detected by tracking of the spacecraft or by observing the pulsar period. Since the

Table 1.1 Overview of prototype laser interferometer antennas in the world and the best sensitivity obtained so far in each group.

INSTITUTE	MIT*	MPI	GLASGOW	CALTECH	ISAS
START	1971	1975	1976	1980	1986
TYPE	DL	DL	FP	FP	DL
ARMLENGTH [m]	1.5	30	10	40	10
REFLECTION NUMBER or FINESSE	50	100	3000	2000	100
TOTAL PATH LENGTH [km]	0.075	3	30	75	1
δl SENSITIVITY at 2 kHz [m/$\sqrt{\text{Hz}}$]	6×10^{-17}	3×10^{-18}	1×10^{-18}	8×10^{-18}	1.6×10^{-17}
STRAIN SENSITIVITY at 2 kHz [1/$\sqrt{\text{Hz}}$]	4×10^{-17}	1×10^{-19}	1×10^{-19}	2×10^{-19}	1.6×10^{-18}

*MIT is now working on a 5 m Fabry-Perot system.

light travel time to spacecraft and pulsars is very long, the experiment is most sensitive to gravitational waves with frequencies in the millihertz range and in the microhertz range, respectively.

Another promising approach is the use of a laser interferometer with which the change in propagation time of light traversing gravitational wave can be measured. The antennas of this kind were first considered in the early 1970s by R. Weiss at MIT [6] and the first experiment has been done by R. Forward at Hughes Research Laboratories [7].

There are many advantages of the interferometer scheme as compared with the bars. The most significant is that the gravitational-wave signal can be easily increased linearly with the arm length of the interferometer antennas just by placing freely suspended test masses at a long distance apart, whereas the bar antennas have rather fixed size. In this sense, the interferometers have much more potential than the bars in terms of sensitivity. For example, whereas the quantum limit due to the uncertainty principle may be hit in the resonator experiment before one reaches the desired sensitivity, it occurs much later in the large interferometer.

It is true that the laser interferometer antennas are at present somewhat less sensitive and less mature than the bar antennas, which have reached a very high level of performance. The current interferometers with armlength of several tens of meters in the world are not actual detectors. They are just prototypes for the study of noise sources and long-term stability to be used in the future for construction of a full sized antenna.

An extensive program for gravitational wave research with km-class large laser interferometers is now being planned in several groups. With such large interfero-

meters one can easily increase the sensitivity of the antennas by factors of 10^2 to 10^3 over that of current prototypes. Assuming there are more advancements or development in technology, another two orders of magnitude of improvement can be expected.

Laboratory scale prototypes with arm lengths extending from 5 m to 40 m are under development at several laboratories around the world to investigate the performance of the interferometer antennas. In chronological order, these are:
(i) Massachusetts Institute of Technology (MIT) [*8*]
(ii) Max Planck Institute für Quantenoptik (MPI) [*9*]
(iii) University of Glasgow [*10*]
(iv) California Institute of Technology (Caltech) [*11*]
(v) Institute of Space and Astronautical Science (ISAS) [*12*]
Table 1.1 shows the current prototypes with best sensitivity attained at each laboratory.

The MIT group contributed significantly to the realization of optical delay lines for achieving long optical paths as well as the use of optical fibers for reducing beam geometrical noise. Although their noise level is still rather high, substantial improvement is expected from the current-developing 5 m prototype.

The MPI group has always lead this field in terms of sensitivity. They also use optical delay lines and have overcome the problem of scattering light accompanied with the delay-line scheme by an elaborate frequency stabilization system, and the problem of beam geometry fluctuations by passing the light through a mode cleaning device. The best sensitivity for strain obtained with their 30 m prototype is $1.1\times10^{-19}/\sqrt{\text{Hz}}$ at 2 kHz.

The prototypes developed at Glasgow and later at Caltech use the Fabry-Perot cavity for long optical paths, which allow smaller mirrors and potentially longer storage times than the delay line scheme [*13*]. The arm length of the Glasgow and the Caltech prototype is 10 m and 40 m, respectively. The sensitivity they achieved are nearly identical to that of the MPI group, although the techniques, the laser powers, and the light storage times differ significantly.

Finally, our group has just started the experiment with our 10 m prototype. We use the delay-line scheme and have made great progress in a very short period of time (see Appendix A). Since we have achieved a sensitivity level sufficient for the further development, we proceeded to investigate long data taking runs.

Long data taking runs with interferometer antennas have been neglected in the past in the development of laser interferometer gravitational wave antennas. This is mainly because the detection of gravitational waves is considered to be very unlikely with the current sensitivity of the interferometer antennas. Thus effort has been concentrated on an improvement of sensitivity rather than data taking. We believe, however, long data taking runs are very significant and it is timely to perform them at present.

The reason is, first of all, that investigation of long-term stability in the interferometer antennas is much behind the progress of the sensitivity of the antenna.

The current interferometer antennas in the world, including our group, are approaching the best sensitivity obtained with the cryogenic resonant bars so far. This

level also corresponds to the strength of the gravitational waves emitted from supernovas in our galaxy.

The bar antennas, however, surpass the interferometer antennas substantially in terms of long data taking runs. The time scales for the cryogenic bar experiments are governed by the long turn-around time caused by cool down and warm up of the bar, which can easily exceed several weeks. In addition, once the bar starts operating, there is little need for making changes in the parameters of the set-up to maintain the system to the best performance.

On the contrary, the interferometers have poor experience in long term operation: the longest continuous run (without any interruption) of the laser interferometer antennas ever done had been only 1–2 hours until our recent more than 5 hour operation. The interferometers are rather complex systems. Our interferometer, for example, has 24 local control systems and two elaborate feedback systems using a modulation technique. Even a trifling trouble on a certain part causes the breakdown of the whole system. Furthermore, the current laser, one of the most important elements in the interferometer, is not stable enough to allow continuous operation for many days or even months. This unbalance of progress between the sensitivity and long-term stability is one of the problems in the interferometer antennas.

Furthermore the long-term stability will be of much more significance in large interferometer antennas in future. The current interferometers with arm lengths of several tens of meter are just prototypes. The complete antenna with an arm length of several kilometers will be more complicated and thus difficult to operate for a long time. We should, however, operate such elaborate systems for months or years continuously to search for gravitational waves in future. Hence it is reasonable to start studying the long-term stability at present for the future large antennas.

Another important aspect of the long data taking runs is analysis of the noise distribution. The storage of the data into computers enables us to analyze the character of the interferometer noise from the standpoint of burst search. The groups engaged in gravitational wave detection using laser interferometers have preferred to represent the performance of their antennas by the average noise spectrum for some extended period. This expression is very useful to analyze rather stationary noises; but it lacks the information of burst-like noises, which can be concealed by taking averages. The burst-like noises are very essential in the interferometer antennas particularly when searching burst waves. Therefore data analysis in this sense is significant and inevitable for future development of the antennas.

Finally it should be emphasized that the possibility of gravitational wave detection should not be totally excluded. The present prototype interferometer can barely detect a supernova which may occur in our galaxy, at best every 10 years. Although the probability is low, it is not absolutely zero. It is also important to set an upper limit value for the intensity of gravitational waves for such astronomical phenomena as SN1987A. Any scientific prediction has not been proved right until it is verified by experiment.

From these various standpoints mentioned above, we performed long-term data taking for more than 100 hours. The main objectives of the long data taking runs are

summarized as follows:

(1) to indentify and, if possible, eliminate key factors which unlock the main feedback or frequency stabilization system;
(2) to study deterioration of the sensitivity by the passage of time;
(3) to obtain and analyze long-term data for non-gaussian noise contributions;
(4) to verify that the data acquisition system works well;
(5) and to find, or to set a practical upper limit for, gravitational wave bursts for a selected period of time.

In this paper, chapter 2 presents the nature of gravitational waves and principle of laser interferometers for detecting gravitational waves together with brief reviews of gravitational wave sources and expected strength of the waves on the earth. The detailed specification of the 10 m prototype for the laser interferometer antenna is described in chapter 3. Chapter 4 summarizes the character of various noise sources in the interferometer antennas. Chapter 5 describes the frequency stabilization system which is especially important for this experiment. Chapter 6 shows the present performance and capability of the 10 m prototype as well as the actual noise behavior. Chapter 7 shows the data acquisition system used, and analyzes the long term stability and noise distribution obtained. Finally, in chapter 8, the conclusion of this experiment and possible future improvement is presented.

2. Gravitational Waves and Laser Interferometer

2.1 Nature of Gravitational Waves

Einstein predicted in his paper from 1918 that gravitational waves are generated by the accelerated motion of masses and propagate as transversal quadrupole waves with the speed of light. Their effect consists in a time-dependent change of the spatial metric. When two free masses are placed in a plane perpendicular to the propagation direction of the wave, the proper distance between two masses, which is defined by the travel time of light is modulated by the gravitational wave (see Appendix B). Assuming a gravitational wave with a particular polarization, the distance variation δl between the two masses is proportional to the natural distance l and the amplitude of the gravitational wave h:

$$\delta l = \frac{1}{2} \mathrm{h} l.$$

The polarity of the effect is opposite for two orthogonal directions, the orientation of which is determined by the polarization of the gravitational wave.

Figure 2.1.1 shows a schematic view of the gravitational-wave-caused change in the geodesic separation between test particles. As a gravitational wave passes, it deforms what was a circle in the proper reference frame into an pulsating ellipse.

2.2 Laser Interferometer for Detecting Gravitational Waves

The travel time of light between two objects in free fall is modulated by gravitational waves as mentioned above. The measureable quantities are the changes

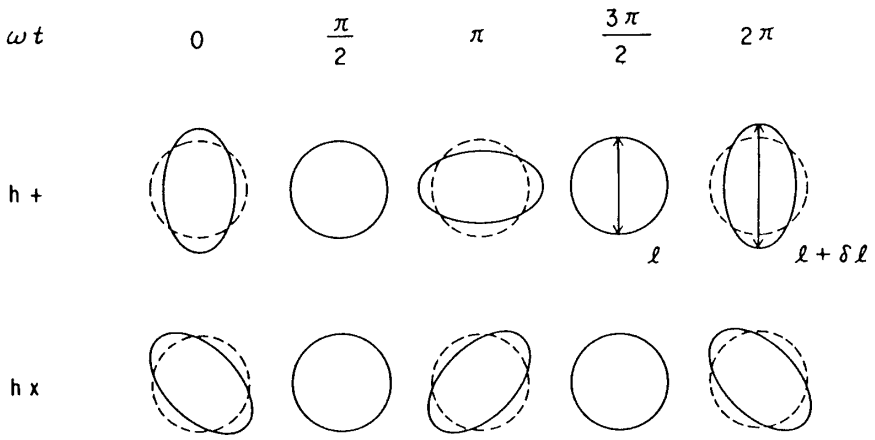

Fig. 2.1.1 Schematic view of the gravitational-wave-caused change in the geodesic separation between test particles. As the gravitational wave (polarization h_+) passes, it deforms what was a circle in the proper reference frame into pulsating ellipse. A wave of polarization $h_\times$ deforms the circle at a 45-degree angle to the axes of h_+.

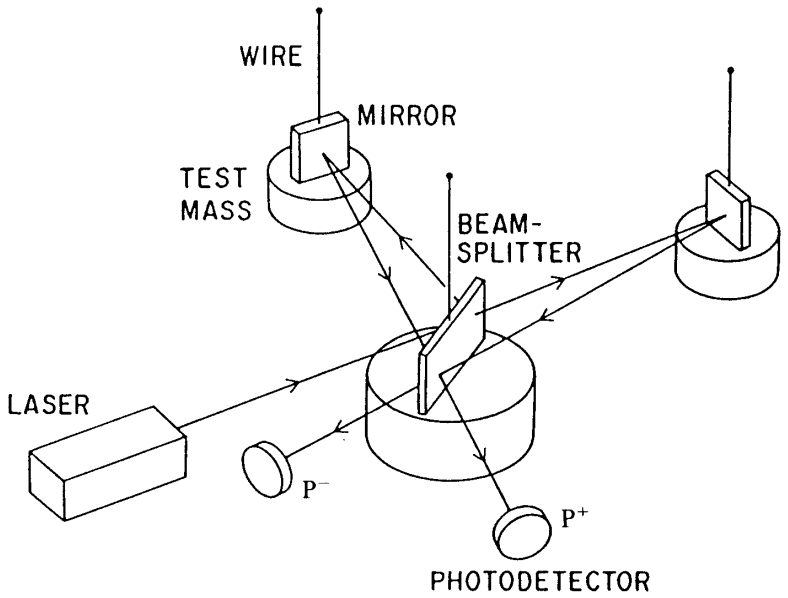

Fig. 2.2.1 Principle of laser interferometer antennas for detecting gravitational waves. Three test masses (two mirrors and a beamsplitter) are suspended like pendulums. The strain caused by gravitational waves can be measured by detecting the intensity change of the interfering light.

in the travel time. It is difficult, however, to measure the travel time absolutely, since strain amplitudes of gravitational waves are expected to be extremely small and there are no time standards accurate enough for such measurement. One possible way to avoid absolute measurement is to measure the difference in travel time of light propagating in two orthogonal directions. The condition that the system be insensitive to clock instability is satisfied by making the two optical paths equal. This can be done

using Michelson interferometers. In this method the time difference is not measured directly but rather the difference in phase of two light beams having traversed the orthogonal paths is measured interferometrically.

As indicated in Fig. 2.2.1, three test masses (a beamsplitter and two mirrors) are placed so as to give two perpendicular optical baselines. A laser beam is divided at the beamsplitter and, after being reflected from the two mirrors at a distance, is re-combined again. One of the interfering beams is detected by a photo-detector to measure the phase difference. Each test mass is suspended by wires like a pendulum; it acts like a free mass for gravitational waves with frequencies much higher than the pendulum frequency.

Such a system of orthogonal reference arms is suitable to the quadruple nature of gravitational waves. Assuming a gravitational wave propagating in the direction perpendicular to the two interferometer arms with polarization axes coinciding with the two arms, the wave affects the two arm distances in the opposite way: when the differential strain in one arm increases, that in the other decreases.

The most outstanding advantage of the interferometer scheme is that the signal-to-noise ratio can be improved substantially by increasing the arm length. While the gravitational-wave signal in the interferometer increases, up to a certain limit, linearly with the arm length, most noises such as laser-originated noises do not depend on the arm length explicitly.

More exactly, the interferometer arms can be made as large as is consistent with the condition that the travel time of light in the arm does not exceed one-half the period of the expected gravitational wave. If the light spends a time longer than half the period, there may be an actual loss of signal. In general, the measurable signal of the path difference variation δL_M may be a portion of the real deviation δL_{GW} caused by the gravitational wave:

$$\delta L_M = \delta L_{GW} \frac{\sin(\pi T_L/T_{GW})}{\pi T_L/T_{GW}},$$

where T_L is light storage time and T_{GW} is the period of the gravitational wave. Since δL_{GW} is proportional to the total pass length L and the light storage time T_L, the measurable signal δL_M can be maximized when

$$T_L = \frac{1}{2} T_{GW}.$$

For example, for the gravitational wave with a center frequency of 1 kHz, the optimum path length is 150 km.

Fig. 2.2.2 shows the response of an interferometer with a fixed arm length for the gravitational wave with different frequencies. It can be seen that the response is flat in low frequencies, and above a corner frequency given by the light storage time, the response follows a 1/f law with notches at multiples of the frequency $f=1/T_L$.

This is the principal feature of laser interferometer antennas relative to bar antennas. The size of the bars is limited by the speed of sound in materials: at most several meters for the 1 kHz gravitational wave.

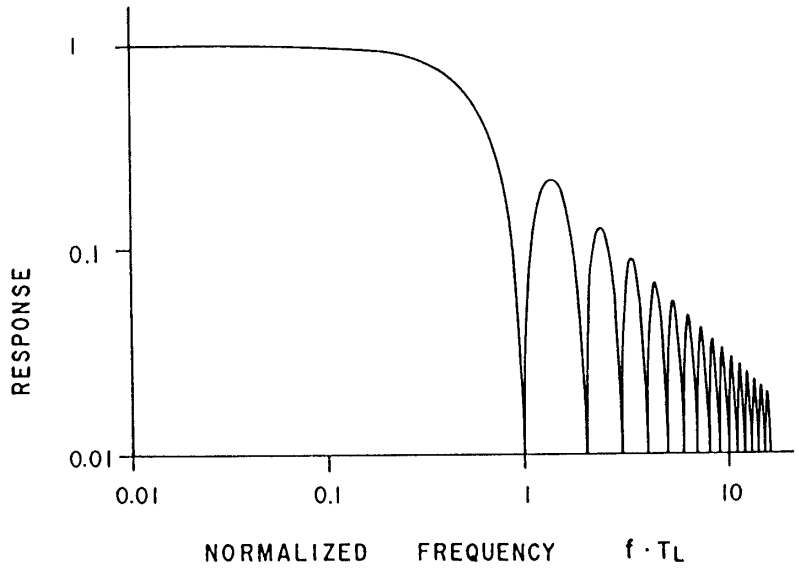

Fig. 2.2.2 Response of Michelson interferometer antennas for gravitational waves. The antenna is assumed to have a fixed total path length. The frequency is normalized with respect to the light storage time T_L.

Another important feature of the interferometer antenna is that it can be operated over a wide range of frequencies and is thus useful in the search for all classes of gravitational-wave sources. Above all, the interferometer antennas are the most effective for gravitational-wave burst search. It is true that the current interferometer antennas are still somewhat less sensitive than the bar antennas. However, interferometer antennas can work in frequency ranges far from the resonance frequencies of bar antennas. Additionally, when the sensitivity of the antennas becomes sufficiently high, the interferometer can follow the time dependent wave shapes of bursts with fidelity and be a powerful diagnostic tool in determining the radiative processes in the sources.

The interferometer antennas are also effective for periodic waves especially with rapidly-varying frequency. Resonant antennas for periodic waves can also follow the frequency drift, but an elaborate technique is required to follow the frequency of the target and the available variation is limited to a very small amount. On the other hand, the interferometer antennas can easily follow large frequency drifts. Any analysis can be performed by computers, once data are taken and stored.

2.3 Sources of Gravitational Waves and Expected Signals

Because it is almost impossible to create on earth a gravitational wave source strong enough to be sensed, we must depend on cosmic sources to excite detectors.

There are three types of gravitational waves from astronomical sources: bursts, continuous waves, and stochastic background (see Appendix C). In any case, gravitational waves are generated by relativistic motions in region of strong gravity.

The most promising sources for burst searches are supernovas and coalescing binaries. It is predicted that the gravitational waves emitted from such sources in our

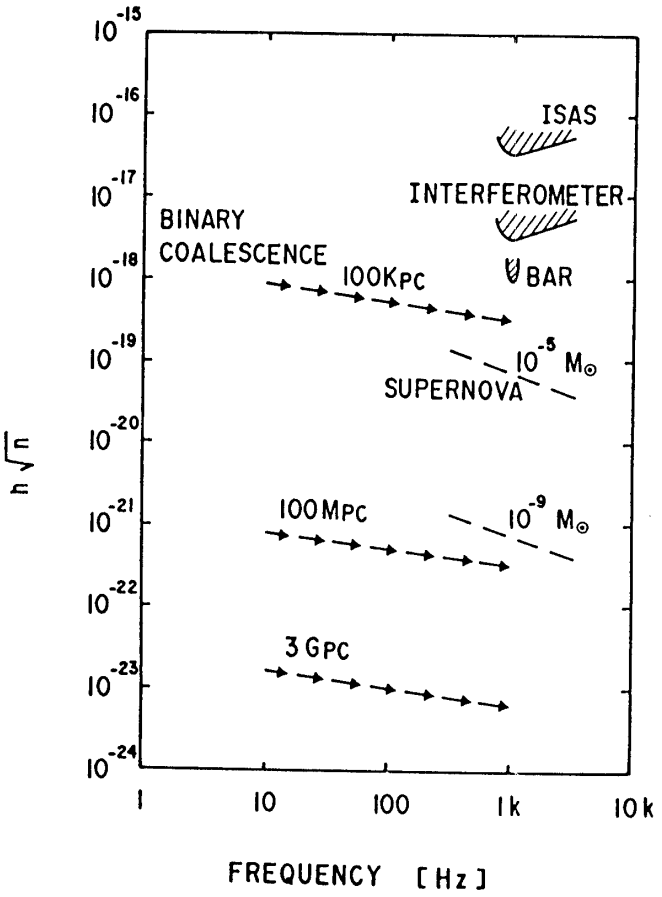

Fig. 2.3.1 Predicted strength of gravitational-wave burst on the earth as well as the current sensitivity of detectors. The strength is expressed as $h\sqrt{n}$, where h is the gravitational-wave strain and n is the number of oscillations observed in the wave train. Supernovas in our galaxy with emitted gravitational-wave energies of 10^{-5} and 10^{-9} $M_\odot$, and the evolution of compact binaries at a distance of 100 kpc, 100 Mpc, and 3 Gpc are indicated.

galaxy have a strain in the order of 10^{-18} to 10^{-19} with a frequency of 100 to 1 kHz on earth. Unfortunately such events in our galaxy are quite infrequent: at best only about one supernova per 10 years may occur. Therefore one must reach out to the Virgo cluster to gain a more frequent event rate, but with much smaller expected strains on earth.

Figure 2.3.1 summarizes the expected gravitational-wave strength on earth from those sources as well as the current best sensitivity of detectors.

3. 10 m Prototype for the Laser Interferometer Antenna

3.1 Principle

A simplified schematic diagram of the 10 m prototype for the laser interferometer

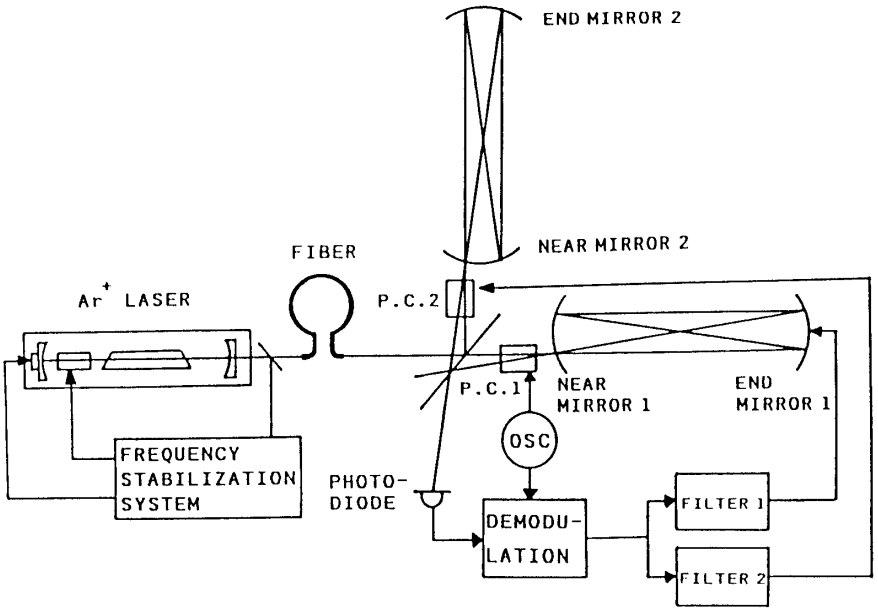

Fig. 3.1.1 Schematic diagram of the 10 m prototype of a laser interferometer gravitational wave antenna. The frequency-stabilized Ar^+ laser, the optical fiber, the two arms of the interferometer with 4 beam delay line, and rf dark-fringe locking system are shown.

antenna is shown in Fig. 3.1.1. It is fundamentally a Michelson interferometer illuminated by Ar^+ laser with folded optical paths. The laser beam enters the vacuum system from outside through a single-mode optical fiber. The beam is divided at a beamsplitter to two perpendicular directions. Each beam passes through a Pockels cell and enters an optical delay line consisting of two spherical mirrors (a near mirror and an end mirror) through a small hole cut in the near mirror. After 102 reflections between the mirrors (in the figure, only 4 reflections are shown), the two beams are re-combined at the beamsplitter. Since the mirror separation is about 10 m, the total optical path is approximately 1 km. This delay line scheme is used to increase the signal caused by gravitational waves.

One of the interferometer outputs is detected with a PIN photodiode outside the vacuum tank. Then the output of the photodetector is converted to the deviation signal from a minimum of intensity (dark fringe) at the detector using a phase modulation technique. This signal is fed back to one Pockels cell and to the driver of one end mirror to hold the interferometer in the dark fringe (rf dark-fringe locking). The locking of the system to the dark fringe is necessary for the reduction of some noises such as shot noise and laser intensity noise.

In such a mode of operation, the feedback signal is proportional to the differential strain induced in the arms. Therefore this signal would contain the gravitational wave signal.

The mirrors and the beamsplitter used are suspended by wires with resonance frequencies (about 0.5 Hz) far below the interesting frequency range for the gravitational wave detection. As a result, we can regard the mirrors and the beamsplitter as free masses for gravitational waves in such a frequency range. The

Table 3.1.1 Specifications of the 10 m prototype laser interferometer antenna (I).

Laser	Type	Ar^+ Laser (GLG 3304, NEC)
	Wavelength	514.5 nm
	Available Power	500 mW (with Etalon and Pockels Cell)
	Mode	Single Transverse Mode Single Longitudinal Mode
Pockels cell	Type	Phase modulator (PM25, Gsänger)
	Crystal	2×ADP 45°y-cut
	Surface Angle	Brewster angle
	Efficiency	2.6×10^{-10} m/V
Optical Fiber	Type	Polarization Maintaining Single Mode Fiber (SM 48-P, Fujikura)
	Length	10 m
	Diameter of Core	3 μm

suspension scheme is also useful for passive isolation from ground motion.

The pendulum mode is damped by applying magnetic forces to the suspended components. It is called local control. This system is indispensable for interference contrast of good quality.

Frequency stabilization of the laser is also an essential part of the whole system. The deviation of the laser frequency from a Fabry-Perot cavity serving as a reference is producing a signal by means of phase modulating the light impinging on the cavity, and by demodulating the light reflected from the cavity. This signal is fed back to a Pockels cell and a piezoelectric transducer of the laser to control the laser cavity length. As a result, the laser frequency is locked to the Fabry-Perot cavity.

Table 3.1.1 shows the specification of the 10 m Prototype for the laser interferometer antenna.

3.2 Laser

An argon ion laser (GLG 3304, NEC) is used with a wavelength of 514.5 nm for illuminating the 10 m laser interferometer. A single longitudinal mode is selected with an etalon inside the cavity. A typical power of the laser with a current of 25 A in multi-mode is 1700 mW and in a single mode 900 mW.

The laser has a pockels cell (PM 25, Gsänger) inside the cavity and a piezoelectric

Table 3.1.1 Specifications of the 10 m prototype laser interferometer antenna (II).

Main Interferometer	Type	Delay Line
	Arm Length	9.86±0.015 m
	Number of Reflections	102
	Total Path Length	1 km
	Method of Measurement	RF Dark-Fringe Locking
Mirror	Radius of Curvature	10.18±0.015 m
	Diameter	ø 160 mm
	Thickness	25 mm
	Diameter of Input Hole	ø 6 mm
	Position of Input Hole	60 mm from Center
	Reflectivity	99.5%
	Material	BK7

transducer (Model 21.938, Lansing) is attached to the fore mirror of the cavity for the purpose of frequency control. With these the laser frequency can be varied by changing the effective length of the laser cavity.

There is some optical loss associated with the use of a Pockels cell inside the cavity, which results in less light power being available. To confine this loss to the minimum, a Pockels cell consisting of two crystals with Brewster's angle is used. Even so, the available power is typically reduced from 900 mW to 500 mW.

The laser sits on a vibration-isolating table with air springs to minimize vibration-induced noise such as frequency fluctuation noise.

3.3 Optical Fiber

A single mode optical fiber (SM 48-P, Fujikura, polarization maintaining), 10 m long with a 3 μm mode diameter, is used to carry the laser light from the laser table into the vacuum. Using this optical fiber, the laser with its mechanical noise originating from the water cooling can be placed on a separate table and thus be isolated from the interferometer.

This special sort of optical fiber can maintain the polarization of the light. If linearly-polarized light is injected into the fiber with the polarization plane of the light

Table 3.1.1 Specifications of the 10 m prototype laser interferometer antenna (III).

Local Control	Test Mass	Bare Mirror
	Suspension Point	2
	Position Sensor	LED and Photodiode
	Actuator	Magnet and Air Coil
Frequency Stabilization	Method	RF Reflection Locking
	Reference	FAbry-Perot Cavity (length: 25 cm, Finesse: 300)
	Actuator	PZT and Pockels Cell in Laser
	Original Frequency Fluctuation	1 kHz/$\sqrt{\text{Hz}}$ at 1 kHz
	Loop Gain	70 dB at 1 kHz
Vacuum System	Pump	Turbo Molecular Pump (2000 *l*/sec)
	Build-Up	10^{-3} mbar in 8 hours

in accordance with that of the fiber, the outgoing light will also become linearly-polarized. Under this condition the polarization of the outgoing beam is insensitive to external stress on the fiber; the vibration of the fiber does not cause any fluctuation of the polarization of the outgoing beam.

An objective lens of a microscope (×20) is used to couple the laser light into the fiber. The fiber input assembly has adjustment capability of 6 degrees of freedom: two translations for positioning, a beam-directional translation for mode matching, two rotations for parallel injection, and a rotation around the fiber axis for polarization adjustment. Precise adjustment permits a maximum transmission efficiency of approximately 50%.

The fiber output assembly, which also uses an objective lens (×20), is mounted on a metal disk similar to the mirrors in size. The disk is then suspended by wires like the mirrors in the interferometer for isolation from ground motion.

The most major advantage of use of the fiber is in its faculty of transverse mode cleaning. The single mode fiber propagates only one mode and loses all others. As a result, the fluctuations in beam geometry can be expected to be suppressed significantly.

The light reflected at the surfaces of the fiber should not enter the laser. Otherwise the optical feedback will hinder the normal operation of the whole system. To avoid this problem, the surfaces of both fiber ends are cut not perpendicularly but with a

little angle.

3.4 Optical Delay Line

The detection sensitivity for the gravitational-wave signal in the interferometers can be increased by increasing the optical path. This is true up to the path length of half the wavelength of the gravitational wave. For example, the optimum optical path for an assumed gravitational wave with a center frequency of 1 kHz is 150 km. Such large interferometers are, however, almost impossible to construct on earth.

One method of achieving longer optical paths is to fold the light many times in the arms using additional mirrors; the gravitational-wave signal can be multiplied by the number of reflections of the light. One disadvantage of this scheme as compared with simply-lengthened arms is that any differential mirror motion, e. g. due to seismic noise or thermal noise, would also be increased together with the gravitational-wave signal.

The laser beam divided at a beamsplitter enters the interferometer arms through holes cut in near mirrors, which are spherical mirrors located close to the beamsplitter. The beam is reflected and refocused by end mirrors, which are also spherical mirrors. The beam continues to bounce back and forth, hitting different parts of the mirrors. Finally, the beam leaves through the same hole it entered—but at a different angle from that on entering. This multi-pass geometry is called an optical delay line [*14*].

In such delay lines, the beam spots on the mirror surface lie on an ellipse in general. With a proper choice of the direction of the incoming beam the spots can be arranged in a circle. The number of transits is determined by the curvature radius of the mirrors R and their separation l (see Appendix D). For example, when arm length equals curvature radius (confocal case), a total number of passes N in the delay line will be four. With a small deviation from the confocal case, we can obtain a considerably larger number of reflections.

In the actual delay line of our interferometer, the separation between mirrors with a curvature radius of 10.18 m is adjusted to 9.86 m so that a reflection number of $N=102$ in the delay line is realized. The total optical path L, N times the arm length l, is therefore approximately 1 km, which corresponds to a delay time of 3.3 μs.

When the outgoing beam leaves the dalay line at exactly the same place it entered the near mirror, the condition is called re-entrance. In this condition, the beam appears to be reflected by the back spherical surface of the near mirror. The outgoing beam is, to first order, insensitive to angle and lateral motions of the end mirrors. Therefore, the requirement for control of the relative angles and positions of the end mirror to the near mirror is not critical.

In general the beam size varies between the different reflection spots. For example, if the incoming beam is focused to the entrance hole, the outgoing beam is again focused to the entrance hole. The expected beam spot size on the mirrors, in this case, is shown in Fig. 3.4.1. The actual diameter of the spot depends on the divergence of the incoming beam and on the distance of the mirrors. In our case the beam waist is located somewhere between the entrance hole and the mid-point of the arm; the

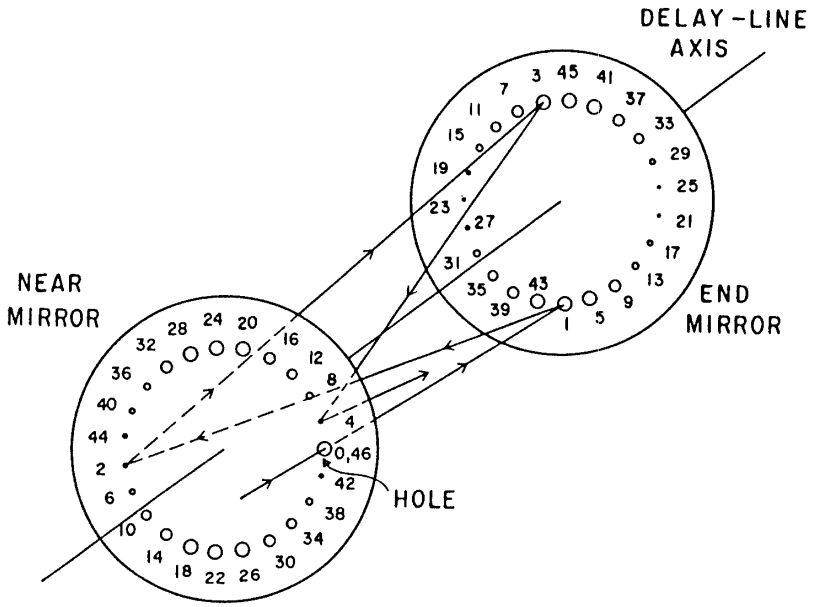

Fig. 3.4.1 Beam spots on the delay-line mirrors with 46 reflections. The order of the spots, the beam size, and the beam pass are indicated.

difference of the spot size is not as larger as in the case when the beam waist is at the entrance hole.

Ideally the delay time of the light should be half a period of the aimed gravitational wave. In reality, however, the reflection number N may be limited by one of two factors: the reflection losses at the mirrors and the size of the mirrors. In the first case, a decrease in the light power by the reflection losses results in a decrease in the signal as well as in the shot noise but with different dependence. While the signal is linear to the available power, the shot noise is proportional to the square root of the power. As a result the optimum sensitivity limited by shot noise is obtained with a reflection number of

$$N_{OPT} = \frac{-2}{\ln R},$$

where R is mirror reflectivity. Since our mirrors have a reflectivity of 0.995, the optimum reflection number N_{OPT} is about 400.

The other factor is the size of the delay line mirrors. One must keep the light from the nearest reflection spot well away from the entrance hole. If one wants to separate the next spot from the entrance hole by, for example, three spot diameters, the maximum number is [*21*]

$$N_{MAX} \simeq \frac{D^2}{12\lambda l},$$

where D is the diameter of mirrors and λ is the wave length of laser light. We use mirrors with D = 160 mm; the maximum number N_{MAX} is about 420. In reality, we

use only 102 reflections to avoid any complexities associated with increases in the reflection numbers.

3.5 Mirror Suspension

In the interferometer antennas, all test masses should act as free masses for the aimed gravitational wave. The most convenient method of forming free masses on earth is simply to suspend the test masses by wires with resonance frequencies (around 1 Hz) far below the interesting frequency range for the gravitational wave (around 1 kHz).

The suspension scheme also provides the most powerful isolation from ground motion. Since the ideal isolation follows $(f_P/f)^2$, where f_P is the resonance frequency of the pendulum, up to 6 orders of magnitude isolation can be expected in the frequency range of 1 kHz.

The bare mirrors themselves are used as test masses, instead of suspending metal blocks onto which the mirrors are mounted. A wire is wrapped around the lower half of the mirror's perimeter. In this suspension scheme, we can avoid complicated mechanical resonances accompanied with complicated mirror mounts [*15*].

The fiber end disk, which has a shape similar to that of the mirrors, is also suspended by wires like the mirrors to reduce beam jitter.

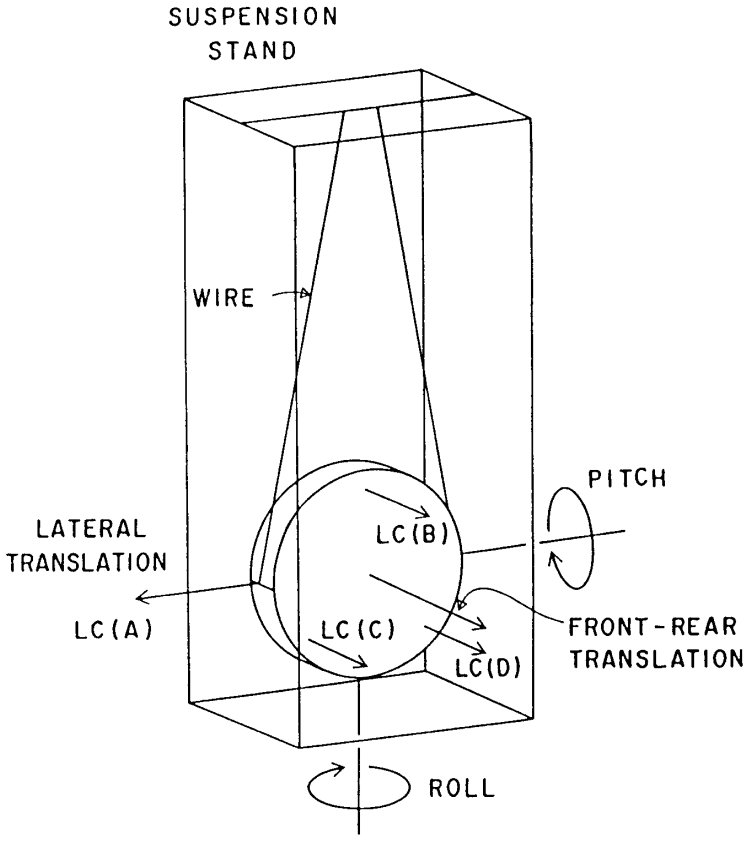

Fig. 3.6.1 Mirror motion—LC(A), LC(B), LC(C), and LC(D)—to be damped by the local control system. Four degrees of freedom of the mirror are also shown.

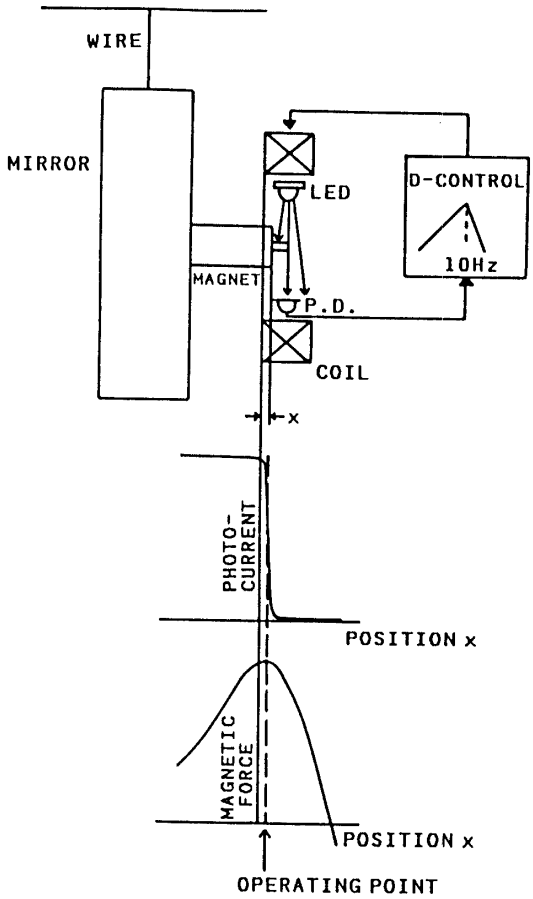

Fig. 3.6.2 Principle of the local control system. The schematic view of the photocurrent of the photodiode and the strength of the magnetic force are indicated in terms of the relative distance between the mirror and the local control unit.

3.6 Local Control

The suspended optical components including the fiber end disk should be damped at low frequencies to prevent large motions due to the ground vibration at the resonant frequency (near 0.5 Hz). Without any control, the pendulum amplitude is enhanced to the order of 10^{-4} m. Such values are totally unacceptable because the direction of the reflected beam fluctuates so much and consequently an interference contrast of good quality cannot be maintained.

Since the optical component is suspended at two points, the four degrees of freedom to be stabilized for each component are pitch, roll, lateral translation, and front-rear translation. Instead of controlling such modes, we control positions of four appropriate points, LC(A), LC(B), LC(C), and LC(D) as shown in Fig. 3.6.1.

Each optical component is hung by wires attached to the individual suspension stands. The relative motion of the component to the suspension stand is sensed and controlled by the local control system. Small plates are mounted on the suspended component for the four positions to be damped independently. An infrared LED and

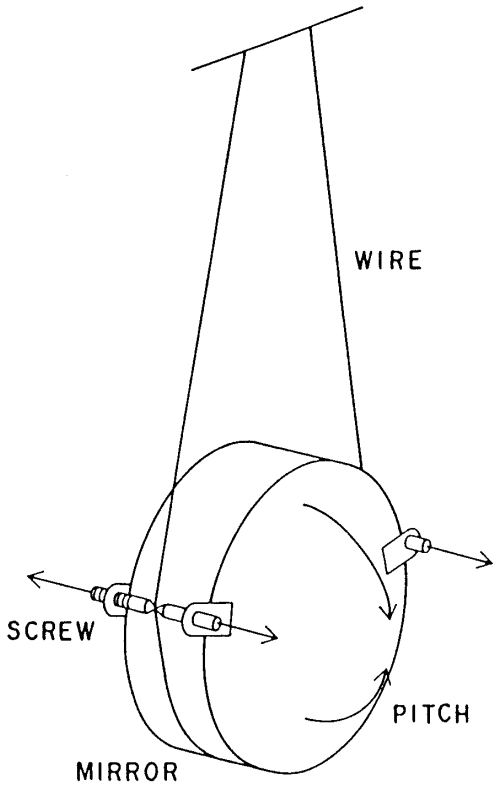

Fig. 3.7.1 Schematic view of the mirror suspension system. The screw translation of the point at which the wires leave the mirror permits a coarse adjustment around the horizontal axis (pitch).

an opposing silicon photodiode are fixed to the suspension stand so that the infrared light emitted from the LED can be interrupted partially by the small plate as shown in Fig. 3.6.2. As a consequence the current in the photodiode can be proportional to the displacement of the small plate. The dynamic range of this sensing system is about 1 mm and the noise in the system corresponds to about 10 nm.

The damping forces are applied by a permanent magnet mounted integrally with the small plate at the suspended component and an air coil mounted concentrically with the LED-photodiode assembly.

The feedback signal is a derivative of the position signal except that the signal rapidly drops off above 10 Hz. This is because the magnetic force applied to the mirror must be small enough in the interesting frequency range (around 1 kHz). The test mass in the interferometer antenna must be a free mass for a gravitational wave with a frequency of around 1 kHz.

The gain of the feedback is set so that the vibration of the mirror caused by an impulse force can be damped after a few bounces.

The relative position of the aircoil to the magnet is set so that the magnetic force exerted on the mirror may be the maximum as shown in Fig. 3.6.2. This results in the best decoupling of the force from vibration of the aircoil induced by ground motion.

Table 3.7.1 Adjustment functions of each optical component.

Optical Component	Motion	Translater
Fiber End Disk	Lateral Translation	DC-Moter
	Vertical Translation	DC-Moter
	Roll	DC-Moter
	Pitch	DC-Moter
	Pitch	Screw
	4-Dimensions	Local Control
Beamsplitter	Front-Rear Translation	DC-Moter
	Roll	DC-Moter
	Pitch	Screw
	4-Dimensions	Local Control
Near Mirror	Roll	Micrometer
	Pitch	Screw
	4-Dimensions	Local Control
End Mirror	Front-Rear Translation	Stepping-Moter
	Roll	Micrometer
	Pitch	Screw
	4-Dimensions	Local Control

3.7 Alignment

Each suspension stand has the function of rotating the suspension point of the pendulum in the horizontal plane. By this function we can adjust the angle of the optical components around the vertical axis (roll). In addition the screw translation of the point at which the wires leave the optical components permits adjustment around the horizontal axis (pitch). Figure 3.7.1 shows the schematic view of this function. This allows coarse alignment of the interferometer in the air.

After the coarse alignment in the air, the whole tank is evacuated, which causes much distortion of the tank itself. As a result, the interferometer becomes totally misaligned. We can compensate for the distortion by adjusting the length of the table leg and of the bellows between the tank and the pipe.

Fine alignment in the vacuum can be accomplished mainly by applying bias currents to the coils that are used for the local control system. While in the local control system the motion of each point to be sensed is damped respectively, we can apply bias currents to the suitable combination of four coils: roll, pitch, lateral translation. Some other remote control systems of the suspension stand such as DC motors and stepping motors are also useful for fine alignment in the vacuum. Table 3.7.1 shows the adjustment function for each optical component. The actual procedure of the alignment is shown in Appendix E.

The precise alignment allows optimization of the contrast in the interferometer. The contrast is defined by

$$C = \frac{I_{MAX} - I_{MIN}}{I_{MAX} + I_{MIN}},$$

where I_{MAX} and I_{MIN} are the photocurrent at the maximum and the minimum of the interference pattern, respectively. The best contrast obtained so far in our interferometer with 102 reflections is C=0.96. The limited contrast is considered to be mainly due to imperfect figure of the delay-line mirrors.

3.8 RF Dark-Fringe Locking

For an ideal adjustment, with parallel wavefronts of the interfering beams, the intensity of the two outputs $P^{\pm}$, which is monitored by two photo-detectors as shown in Fig. 2.2.1, varies as

$$P^{\pm} = \frac{P_0}{2}(1 \pm \cos \Delta\emptyset),$$

with

$$\Delta\emptyset = \frac{2\pi \Delta L}{\lambda},$$

where P_0 is the maximum intensity at the photodiode, $\Delta\emptyset$ and ΔL are the phase difference and the path difference between two arms, respectively, and λ is the wavelength of the laser light.

In the first experiment of the laser interferometer antennas performed by R. Forward, the system was locked to the point of equal intensity in the two outputs [7]. He used the difference signal between two photo-detectors as the deviation signal from the operating point to cancel the intensity fluctuation of the incident laser light. The method now universally adopted is, however, to lock the system to minimum light power in one of the output ports (for example P^-) using the high-frequency phase modulation technique (rf dark-fringe locking) initiated by R. Weiss [6].

The advantages of this method is as follows:

(1) The low light power in the measuring photodiode makes the requirement for the photodiode much easier.
(2) The other interference output, which is locked to maximum light power, can be used to increase the effective light power in the interferometer (recycling).
(3) By high frequency modulation, the fringe signals are placed at frequencies where the laser intensity fluctuation is limited by the shot noise level.

The principle of this rf dark-fringe locking on the basis of our experiment is as follows (ref. Fig. 3.8.1). A phase modulation is impressed on the beam in one arm by applying radio-frequency sinusoidal voltages (9 MHz) to a Pockels cell located just before the near mirror (PC1 in Fig. 3. 1. 1). The resulting phase difference $\Delta\emptyset$ between two arms is

$$\Delta\emptyset = \Delta\emptyset_{ST} + \Delta\emptyset_{NF} + \delta\emptyset_{GW} + m \sin \omega_m t,$$

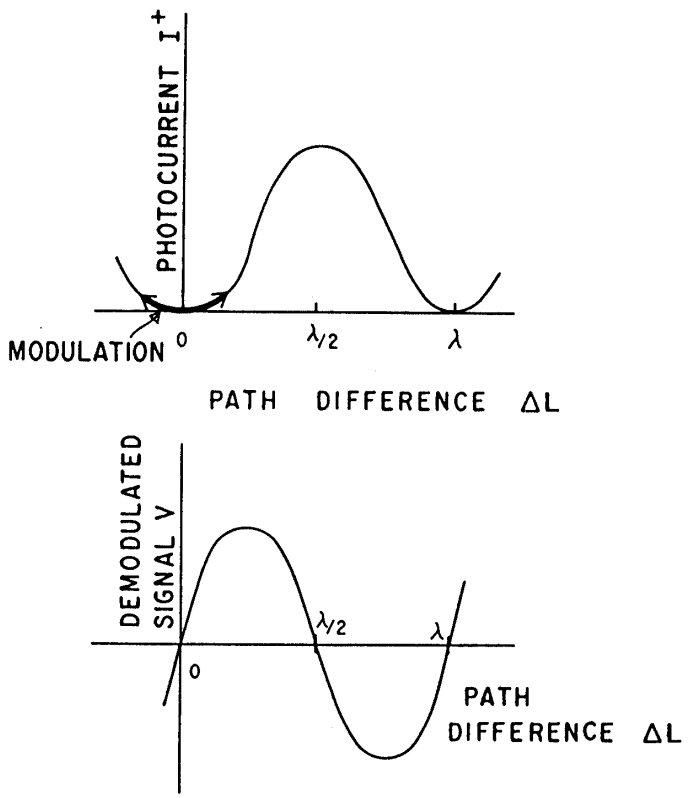

Fig. 3.8.1 Photocurrent of the photo-detector in the interferometer output and the demodulated signal in terms of path difference. The modulation at the dark fringe is indicated.

where $\delta\varnothing_{GW}$ is the phase difference change caused by the gravitational wave, m the amplitude of the phase modulation, and ω_m the modulation frequency. $\Delta\varnothing_{ST}$ is defined to be a static phase difference between two arms, supposing the interferometer is perfectly locked to a particular dark fringe at one of the outputs $P^{\pm}$. Therefore $\Delta\varnothing_{ST}$ must be a multiple of 2π. On the other hand $\Delta\varnothing_{NF}$ is a naturally fluctuating phase difference deviating from this particular dark fringe; $\Delta\varnothing_{NF}$ can be suppressed by the feedback control.

The output of the photodetector contains signals at the modulation frequency and its harmonics. Near the dark fringe in the output P^-:

$$\Delta\varnothing_{NF} << 1,$$

the photocurrent of the modulation-frequency component $I_{\omega m}$ is proportional to the deviation from a dark fringe, and its phase indicates the direction of the deviation:

$$I_{\omega m}=I_0\ J_1(m)\ (\Delta\varnothing_{NF}+\delta\varnothing)\ \sin\ \omega_m\ t,$$

where I_0 is the maximum photocurrent and $J_1(m)$ is the first order Bessel function. This signal is demodulated to recover the original information about the phase

deviation from the dark fringe.

There are two paths in the feedback loops. One is a Pockels cell path and the other is a magnet-coil path. The demodulated signal is high-pass filtered, amplified and then fed back to the second Pockels cell (P.C. 2 in Fig. 3.1.1) to lock the system to a certain dark fringe. Although the Pockels cell has a fast response, its limited dynamic range prohibits the use of only the Pockels cell for this feedback system. Because of the limited drive voltage available, the Pockels cell cannot change the effective path length by more than half a wavelength, while the original fluctuation of the path difference in low frequency is tens of micrometers around 1 Hz. For the other path, the low-pass filtered signal is fed back to the magnet-coil system of one end mirror which is used for the local control system to push and pull the end mirror directly. The local control system has a sufficient dynamic range ($\simeq$1 mm) to correct the large low-frequency fluctuations.

The unity gain frequency of the feedback loop should be substantially high for two reasons. First, as will be mentioned later, the open loop gain below 0.5 Hz must be high enough to eliminate laser intensity noise, which can be ensured by attaining high unity gain frequency. Secondly, in the range where the loop gain is rather high, the feedback signal can cancel all deviations caused in the intereferometer. As a result, the voltage applied to the Pockels cell can be regarded as a linear function of the

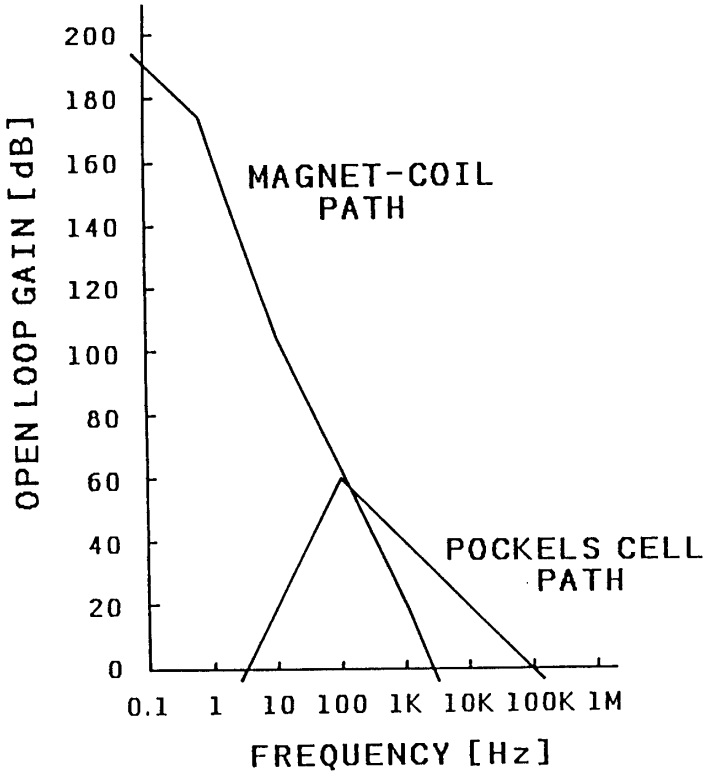

Fig. 3.8.2 Schematic view of the open loop gain in the main feedback system. The magnet-coil path and the Pockels cell path are shown, provided that the gain of the local control system is adjusted to the critical damping.

path-length change, including gravitational wave signals. In the actual feedback loop the unity gain frequency is set to approximately 100 kHz. This frequency is limited by the combination between the −20 dB/decade slope of the Pockels cell path and the rather long time delay (3.3 μsec) due to the passage of the light through the delay line before the second passage through the Pockels cell.

Figure 3.8.2 indicates the open loop gain of both the Pockels cell path and the magnet-coil path, assuming that the local control system causes critical damping (i.e. no resonance peak around the pendulum frequency in the locally-controlled pendulum). As shown in the figure, the cross-over frequency between the two paths is about 100 Hz and the loop gain frequency between the two paths is about 100 Hz and the loop gain near the resonance frequency of the pendulum is approximately 170 dB. The details about the rf dark-fringe locking will be described in appendix F.

3.9 Vacuum System

A vacuum system is absolutely necessary for this sensitive experiment to protect the instrument from acoustic noise and dust. In addition, the phase fluctuation of the beam due to refractive index fluctuations of the air can be considerably reduced by evacuation.

Most parts of the interferometer, after the optical fiber, are contained in a vacuum system. There are three vertical tanks: a central tank, 1.5 m in diameter and 2.0 m in height; and two end tanks, 0.6 m in diameter and 2.0 m in height. The central tank houses the fiber end block, the beamsplitter, two near mirrors, and two Pockels cells, while the end tanks contain the end mirrors. The central tank is connected to the two end tanks by 0.4 m diameter horizontal pipes. The whole system rests on vibration-isolating tables with air spring suspensions. The three tanks and four midway points of the pipe sit on separate tables.

A rotary pump (1200 *l*/min) and a turbomolecular pump (2000 *l*/sec) are used, which allow the system to be pumped from atmospheric pressure to below 10^{-4} mbar in 3 hours. The pressure below 10^{-3} mbar can be maintained for 8 hours after the pumps are turned off. The interferometer is operated during this period to avoid vibration noises from the pumps.

3.10 Frequency Stabilization

A detailed description of the frequency stabilization is given in chapter 5 together with a discussion of its necessity and of the noise caused by laser frequency fluctuations.

4. Noise in Laser Interferometers

4.1 Shot Noise

The most fundamental limit to the sensitivity is set by the quantum uncertainty in the position of the test masses. For a detection of change in position over a time τ, the smallest displacement change detectable is approximately

$$\delta x = \sqrt{2\hbar\tau/M},$$

where M is the mass of the test masses. Assuming 3 km baselines and 100 kg mass, the limitation for the displacement change in a millisecond measurement is

$$h \simeq 1 \times 10^{-23},$$

in terms of gravitational wave amplitude h. This value is small enough to detect the expected gravitational wave signals from the Virgo cluster. Even our prototype of antenna (l=10 m, M=1kg) has a rather small quantum limit,

$$h \simeq 5 \times 10^{-20}.$$

Thus, in contrast to the bar antennas, the quantum limit due to uncertainty principle is not very critical in the interferometer antennas, particularly with long baselines.

In practice, photon-counting error sets a more severe limit on the interferometer antennas. This noise is based on the quantum nature of the light. Since the motion induced by the gravitational wave is small as compared with the laser wavelength, only small changes in the intensity of the interfering light can be expected. On the other hand, any light, which can be regarded as a photon flux, suffers an intensity fluctuation due to photon counting statistics (shot noise). Hence this fluctuation will set the limitation for the measurement of intensity changes.

In the Michelson interferometers, the displacement sensitivity set by the photon counting error depends on the operating point in the interference pattern; i.e. the initial phase difference between two beams. The interferometers are locked to the dark fringe to reduce the shot noise. An alternative mode of operation, the differential method using two photodetectors, provides the same shot-noise limited sensitivity.

The shot-noise limited sensitivity of a Michelson interferometer can be improved by increasing the circulating light power. While the gravitational-wave signal increases linearly with the available light power, the fluctuation due to photon counting error is proportional to the square root of the light power. When we increase the light power, the uncorrelated light pressure fluctuation on the mirrors also increases and finally exceeds the shot noise. With a light power that provides the same amount of both the shot noise and the radiation pressure noise, one can attain the quantum limit due to the uncertainty principle. At present, however, the normal light powers available are sufficiently low so that the shot noise is expected to dominate the radiation pressure noise. For this reason, we will concentrate our attention on the study of the shot noise.

The shot noise limit does not depend explicitly on the number of reflections in the delay lines, whereas the radiation pressure noise does. It is possible to improve signal-to-noise-ratio in interferometers with limited light powers using a multi-reflection scheme such as the delay line.

The shot noise represents a white noise and corresponds to an apparent path difference δL_{SH},

$$\delta L_{SH}=\sqrt{\hbar c\lambda/\pi\eta P}=\frac{\lambda}{2\pi}\sqrt{2e/I},$$

where $\hbar$ is Planck's constant, c the velocity of light, λ the wavelength of the laser light, P the light power available at the interferometer ouptut, η the quantum efficiency of the photodiode, e the elementary charge, and I the photocurrent. This equation is represented in terms of the linear spectral density, which is very convenient for expressing various noises in the interferometer antenna (see Appendix G). As an example, for 10 mW light at 514.5 nm and a photodiode with quantum efficiency of 0.5, the shot noise will be 10^{-15} m/$\sqrt{\text{Hz}}$.

In the actual configuration, however, this limitation is deteriorated because of imperfect interference. The actual limitation can be written in the form [9]

$$\delta L_{SH}=\frac{\lambda\sqrt{eI_{dc}}}{\pi J_1(m)I_{eff}},$$

with

$$I_{eff}=I_{max}-I_{min},$$

$$I_{dc}=I_{min}+\frac{I_{eff}}{2}(1-J_0(m)),$$

where I_{max} and I_{min} are the currents in the measurement photodiode at maximum and at minimum, respectively, $J_0(m)$ and $J_1(m)$ are the zeroth and the first order Bessel functions, respectively, and m is the modulation index. These formulas indicate that there exists an optimum modulation depth which provides the best shot noise limited sensitivity under a particular contrast of interference. For the perfect contrast, infinitesimal modulation index is the optimum, and for a contrast of 92%, which is a typical value in our interferometer, a modulation index of m=1.10 provides the best sensitivity.

For the typical value in our experiment with I_{max}=8 mA, K=92%, and m=0.45, the shot noise level in terms of the path difference is

$$\delta L_{SH}=8.9\times10^{-16}\ \text{m}/\sqrt{\text{Hz}}.$$

This is 4.9 dB (1.8 times) greater than the ideal shot noise with perfect contrast (5.1×10^{-16} m/$\sqrt{\text{Hz}}$).

Although the reduction of the shot noise is a very important goal, our current investigations are focused on identification and elimination of various other noise sources which may exceed the present typical shot noise level. Thus, in the following chapter, we will estimate the various noise effects with shot noise as a reference.

4.2 Laser Intensity Noise

In the frequency range of interest (around 1 kHz), the intensity fluctuation of the argon laser is several orders of magnitude above the shot noise level. Such fluctuations

in the incident laser power can be cancelled in the output of the interferometers using nulling methods such as rf dark-fringe locking techniques. The signal induced by a gravitational wave is linear to the fringe deviation from a certain dark fringe, while the intensity fluctuation is proportional to the intensity itself, thus the square of the fringe deviation. As a result, operation at the dark fringe can totally eliminate the effect of the intensity fluctuation. In reality there is some residual fringe deviation, which may make the intensity fluctuation apparent in the interferometer output. The intensity noise in terms of path differences, δL_{IN}, can be expressed as

$$\delta L_{IN} = \Delta L_R \frac{\delta I}{I},$$

where $\delta I/I$ is the intensity fluctuation of the laser and ΔL_R is the residual deviation from the dark fringe when locking. If there is no offset in the loop, ΔL_R is roughly the original deviation from the dark fringe divided by the open loop gain of the feedback system.

Assuming that the laser intensity fluctuation is $10^{-4}/\sqrt{\text{Hz}}$ and the path difference fluctuation is 50 μm around 1 Hz, the feedback loop gain of 5×10^6 around 1 Hz permits the reduction of the laser intensity noise to the shot noise level.

4.3 Laser Frequency Noise

One of the significant features of the interferometer antenna is that a perfectly constant frequency reference is not required, since the two arm lengths of the interferometer are equal to a high precision; the frequency fluctuation of the incident laser is made apparent in the output of the interferometers only by unequal path lengths in the interferometer. If the path lengths in two arms are different by a static offset ΔL_{ST}, this directly translates frequency fluctuation $\delta\nu$ into apparent signal δL_{FR} in the interferometer output,

$$\delta L_{FR} = \Delta L_{ST} \frac{\delta\nu}{\nu}.$$

Although simple Michelson interferometers with no delay lines can be easily adjusted so that the path difference in two arms may disappear, it is difficult to satisfy the condition in the interferometers with a large number of reflections in delay lines. This is because even a small change in the mirror separation may cause a large motion of the outgoing beam and then violate the re-entrance condition. For the actual set-up with 102 reflections in the delay line, only 1 mm change in arm length causes vertical translations of the outgoing beam by approximately 0.6 mm; under such conditions good interference contrast cannot be expected. Unfortunately the mean curvature of one delay line used for our interferometer differs from that of the other by approximately 10 mm. Thus we cannot cancel the path difference between the two arms without causing deterioration to the interference contrast.

The scattered light may also mimic signals in connection with frequency fluctuations of the laser light, because the scattered light would have totally different path length from the main beam when detected at the photo-detector. This effect will be analyzed

in detail in chapter 4.5.

4.4 Laser Beam Geometrical Noise

A totally symmetric interferometer would be insensitive to geometrical fluctuations of the illuminating laser beam, because the two beams experience the same changes. In the actual interferometer, however, there will be imperfections of symmetry, which lead to the sensitivity to change due to the beam position and direction. In general, the interferometer noise due to such fluctuations tends to be proportional to the degree of remaining asymmetry in the system. For example, if the beamsplitter plane deviates by a small angle $\Delta\theta_{BS}$ from the plane of symmetry in the interferometer, the lateral jitter of the laser beam δx can be translated into a spurious signal δL_{BJ},

$$\delta L_{BJ}=4\Delta\theta_{BS}\ \delta x.$$

The laser geometrical fluctuation can be reduced significantly using optical fibers. Moreover the fiber end assembly is mounted on the disk which is suspended by wires for isolation from ground motion. As a result, a precise alignment of the interferometer is sufficient to suppress this sort of noise in the interferometer output to below the current shot noise level.

4.5 Scattered Light Noise

One of the critical limiting factors in the delay-line type interferometers is scattered light noise. The scattered light can find its way to the photo-detector in the output port with a path length different from that of the main beam. Although the intensity of the scattered light is very low, the interferometer noise caused by the scattered light can be substantial, because of its large path difference to the main beam.

There are many components which can scatter the main beam: Pockels cells, the mirrors themselves, and the inner surface of the vacuum chamber. Among them, the strongest contributions are a result of additional full round trips of scattered light in the delay line. In this case, the path difference between the scattered light and the main beam is a multiple of the delay-line path. Contributions even from light which experiences many round trips can be considerably large due to the high reflectivity of the delay-line mirrors.

For the analysis of the scattered light effect, we assume that only one scattered light component with a certain path difference exists in the interferometer. Let σ be a relative field strength of the scattered light to the main beam—a relative intensity σ^2. Then let $\emptyset(t)$ be the phase difference between the scattered light and the main beam. For $\sigma << 1$, the resulting alteration $\Psi(t)$ of the phase of the main beam due to superposition of the scattered light on the main beam is given by,

$$\Psi(t)=\sigma\ \sin\ \emptyset(t).$$

The phase difference $\emptyset(t)$ depends on the path difference, denoted by $L_{SC}(t)$, between the scattered light and the main beam. If we consider frequency variations

which are slow as compared with the travel-time difference between the scattered light and the main beam, the phase error $\varnothing(t)$ can be expressed by

$$\varnothing(t)=\frac{2\pi \Delta L_{SC}(t)\ \nu(t)}{c}.$$

These equations show that there are mainly two ways in which the scattered light can become apparent in the output of the interferometer. One is due to a fast fluctuation of the frequency $\nu(t)$ or the path difference $\Delta L_{SC}(t)$, and the other is an up-conversion of the slow variations of the phase difference $\varnothing(t)$, through non-linear relationship between the phase difference $\varnothing(t)$ and the phase error $\Psi(t)$.

A rapid change of the phase difference $\varnothing(t)$ caused by the frequency fluctuation $\delta\nu$ or path difference fluctuation $\delta(\Delta L_{SC})$ results also in rapid change of the phase error $\Psi(t)$, which appears as mimic signals in the output of the interferometer. As a result, the interferometer noise of this type, in average, is given as follows:
(i) the frequency fluctuation $\delta\nu$ causes

$$\delta L_{S\nu} \simeq \sigma\ \Delta L_{SC}\frac{\delta\nu}{\nu},$$

(ii) and the path difference fluctuation $\delta(\Delta L_{SC})$ causes

$$\delta L_{SL} \simeq \sigma\ \delta(\Delta L_{SC}).$$

There is, in principle, a method with which we can suppress the above noises. The effect of those noises depend on the mean phase angle $\varnothing_0$. If this angle could be kept at $\varnothing_0=\pi/2 \bmod \pi$, the effect would be cancelled. But in practice, it is difficult to set the condition for all the scattered light with different mean phase angles.

For case (i), we can reduce the noise by stabilizing the laser frequency or reducing the amplitude of the scattered light. Compared with the equation which gives frequency noise due to a static path difference δL_{FR}

$$\delta L_{FR}=\Delta L_{ST}\frac{\delta\nu}{\nu},$$

the scattered light noise $\delta L_{S\nu}$ appears to be reduced by the factor σ, but the path difference ΔL_{SC} can be much larger than ΔL_{ST}.

We can neglect the type (ii) noise for the scattered light from the suspended mirrors. For example, for the scattered light with ΔL_{SC} of one full round trip, $\delta(\Delta L_{SC})$ is almost the same as the normal seismic noise of the interferometer and σ is much smaller than 1, which results in this type of noise being much smaller than the seismic noise.

The light scattered from non-isolated components, such as inner surfaces of the pipe, may cause large type (ii) noise, because $\delta(\Delta L_{SC})$ is still large enough. For the light scattered only once by non-isolated materials, $\delta(\Delta L_{SC})$ should be almost the same as the ground motion, which is approximately 10^{-12} m/$\sqrt{\text{Hz}}$ around 1 kHz. If this sort of scattered light noise has a relative amplitude σ larger than 10^{-3}, the

resulting noise will exceed the current shot noise level.

The other kind of the scattered light noise is up-conversion noise of a slow fluctuation of $\Delta L_{SC}(t)\nu(t)/c$. For example, slow (around 1 Hz) but rather large fluctuation of ΔL_{SC} (1000 λ) causes the phase error $\Psi(t)$ to oscillate 1000 times a second. As a result, the up-converted noise occurs at 1 kHz in the interferometer output.

One method for making this effect clear is to move one of the end mirrors at a constant speed with the help of the local control system. Because of the interferometer locking system, the other end mirror will follow to keep the output on a dark fringe; thus noise measurements are still possible. At this time, the resulting noise spectrum of the interferometer output must have a corresponding up-conversion noise of the scattered light.

There are various ways to reduce the up-conversion noise of the scattered light noise. The easiest is to install black rings around the holes in the near mirrors so as to reduce scattering from beam scraping the edges. Another more effective scheme is to control the path length absolutely so that the path difference between the main beam and the scattered light may be fixed. This has been already done in MPI and good results were obtained [*16*].

4.6 Seismic Noise

The amplitude and frequency spectrum of seismic noise are very dependent on the specific location of the detector site. Most of the seismic measurements indicate that the absolute ground motion decreases with increasing frequency, which can be roughly approximated by a f^{-2} law for the linear measure. The linear spectral intensity of the ground motion is normally

$$\delta x = \frac{10^{-6} \sim 10^{-8}}{f^2} \mathrm{m}/\sqrt{\mathrm{Hz}}\,.$$

We also measured the motion of the floor where our interferometer is located. Though the accelerometer available is not sensitive enough, we were able to set the upper limit for the ground motion:

$$\delta x < 10^{-6}\ f^{-2}\ \mathrm{m}/\sqrt{\mathrm{Hz}}\,.$$

If the mirrors of the interferometer were firmly attached to the ground, the seismic noise would be $\delta L < 10^{-10}\ \mathrm{m}/\sqrt{\mathrm{Hz}}$ at 1 kHz, because of the 102 reflections. This value is much larger than the current shot noise.

Inside our frequency window, around 1 kHz, an effective isolation from ground motion is a pendulum suspension of the mirrors. In the ideal case, the isolation due to suspension is $(f_0/f)^2$ in high frequencies, where f_0 is the resonance frequency of the pendulum. In reality, however, the transfer function exhibits a complex resonant structure above the first resonsnce of the wire used for the suspension. In addition, the finite Q value of the pendulum motion also deteriorates the ideal transfer function of the pendulum (see Appendix H). Consequently it is safe to estimate this isolation not

at 10^{-6} but rather at 10^{-4} around 1 kHz.

In addition to the pendulum method, we isolate the suspension points by rubber rings and put the base plate on rubber. An additional isolation of at least a factor of 10^{-2} can be obtained by proper use of rubber isolations. Consequently the seismic noise would be at most 10^{-16} m/$\sqrt{\text{Hz}}$ around 1kHz, which is a tolerable value in view of the shot noise limit.

There exists another noise caused by ground motion in connection with the local control system. The relative position of the aircoil with respect to the magnet vibrates from ground motion and, as a result, a magnetic force can be exerted on the mirrors. To avoid this effect, we set the aircoil in such a way that the magnetic force exerted on the mirror is maximized; this results in the best decoupling of the force from vibration of the aircoil induced by ground motion. In our case, assuming an error in the coil position of 1 mm and the available bias current, the ground motion could cause mirror motions of a maximum of 10^{-25} m/$\sqrt{\text{Hz}}$ around 1 kHz, which is a negligible level for the current shot noise.

4.7 Thermal Noise

Mechanical thermal noise enters the interferometer in two ways: first, thermal motion of the mirrors as pendulum and second thermal excitation of the internal modes of the mirrors. In either case the mirrors are subject to thermal vibrations with kinetic energies of kT/2 even if the mirrors are completely isolated from ground motion.

As for the pendulum mode, the suspension has a resonant frequency much lower than the frequency of the gravitational wave that is to be detected. In this case, the thermal noise corresponding to mirror motion is given by

$$\delta x_{PE}=\frac{1}{f^2}\sqrt{kTf_0/2\pi^3MQ},$$

where M is the mass of the mirror, Q is the mechanical quality factor, and f_0 is the resonant frequency of the mirror. We measured the Q value of the pendulum by observing the mirror motion damping slowly with the local control off, which resulted in a Q value of 10^3. For this value and the actual number used (M=1.2 kg, f_0=0.5 Hz), we can obtain δx_{PE}

$$\delta x_{PE}=1.6\times10^{-13}\ f^{-2}\ \text{m}/\sqrt{\text{Hz}}.$$

Thus the corresponding path difference noise at 1 kHz is

$$\delta L_{PE}=1.6\times10^{-17}\ \text{m}/\sqrt{\text{Hz}}.$$

This value is low enough as compared with the shot noise.

On the other hand, the resonant peak of the internal mode is

$$\delta x_{IN}=\sqrt{kTQ/2\pi^3Mf_0^3}.$$

For the reasonable values of $Q=10^3$, $M=1.2$ kg, and $f_0=5$ kHz, the noise at the resonance becomes

$$\delta x_{IN}=2.1\times10^{-15} \text{ m}.$$

Since this value is too much for the aimed sensitivity, it is clear that any mode of the internal motions of the mirrors should be higher than the gravitational wave frequency. In this case, below the resonance frequency of the mirrors, the thermal vibrations appear as white noise with a linear spectral density,

$$\delta x_{IN}=\sqrt{kT/2\pi^3 MQf_0^3}.$$

The thermal noise can be, therefore, minimized using high-Q materials for the mirrors and high-Q suspensions.

The delay-line mirrors are made of circular substrates with a diameter of 160 mm and a thickness of 25 mm. For such plates with a small thickness-to-radius ratio, the lowest mode of the plate is the flexural mode with two diametric nodal lines and no circular nodal lines [*17*]. The frequency of the mode is given by

$$f=\frac{1.55}{2\pi}\frac{d}{a^2}\sqrt{E/\rho},$$

where E is the modulus of elasticity, ρ the mass density, d the thickness, and a the radius. For our present mirrors, the frequency is 5.5 kHz.

The Q of the mirrors is limited by the clips at which the wires leave the mirrors. Assuming a rather poor value of 10^3 as Q, we can calculate this noise in terms of the path difference, which is given by

$$\delta x_{IN}=6\times10^{-19} \text{ m}/\sqrt{\text{Hz}}$$

This value is also smaller than the current shot noise.

4.8 Gas Pressure Noise

The optical components for the interferometer after the fiber are contained in a vacuum system to reduce acoustic noise and protect the light path from dust. In addition, the vacuum system is absolutely necessary to suppress the more critical noise which comes from the refractive index fluctuations of the rest gas.

Random fluctuations in the number of molecules in the light path result in fluctuations in the index of refraction of the gas. This causes phase fluctuations of the laser light as it propagates back and forth between delay-line mirrors. The linear spectral intensity of this residual gas noise is given by

$$\delta L_{GA}=\left[\frac{2\sqrt{3\pi}(n_0-1)^2\sqrt{l}}{(A_0/V_0)c_0\sqrt{\lambda N}}(p/p_0)(T_0/T)^{3/2}\right]^{1/2},$$

where A_0 is Avogadoro's number, V_0 the volume of one mole of gas at STP, n_0 the

index of refraction of the gas, c_0 the most probable thermal molecular speed in the gas, p_0 the standard pressure, and T_0 the standard temperature [9].

We usually operate the interferometer with a vacuum of 10^{-3} mbar, which results in the corresponding residual gas noise,

$$\delta L_{GA}=5.0\times10^{-18}\ \mathrm{m}/\sqrt{\mathrm{Hz}}.$$

This noise level is negligible for the current shot noise.

4.9 Electrical Noise

Electrical noise is trivial in principle but rather difficult to eliminate. There are various ways in which the electrical noise becomes apparent in the interferometer output.

In the main feedback loop, the most critical noise is in the preamplifier of the photodiode (O/E preamplifier), while noise produced by electrical circuits after the preamplifier can be easily suppressed below the noise level of the O/E preamplifier. The main noise source in the O/E preamplifier is Johnson noise of the resistance used in the circuit. This noise can be characterized as an additional fixed imaginary current I_{DET} in the photodiode in such a way that the shot noise caused by this imaginary current I_{DET} may be the same as the actual electrical noise.

Figure 4.9.1 shows the method to measure the I_{DET}. First the noise level in the demodulated signal is measured without any light on the photodiode. This noise can be considered as totally due to the electrical noise. Then, using an incandescent lamp, the intensity noise which is only shot noise around 9 MHz, the photodiode is illuminated in such a way that the resultant noise is increased by 3 dB. The I_{DET} is the current of the photodiode at that light level.

Since the electrical noise in the O/E preamplifier is independent of the strength of the incident light, the resulting noise in terms of path difference δL_{EL} depends on not

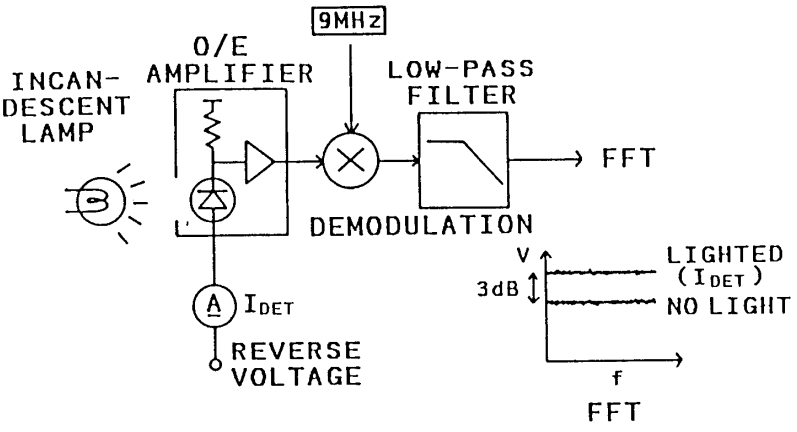

Fig. 4.9.1 Method to measure the equivalent photocurrent of the electrical noise in the O/E preamplifier. When the incandescent lamp causes a photocurrent of I_{DET}, the noise in the demodulation output will be increased by 3 dB.

only the light power but also the interference contrast. We can obtain the following representation by the same way as estimation of the shot noise [9]:

$$\delta L_{EL}=\frac{\lambda\sqrt{eI_{DET}}}{\pi J_1(m)I_{EFF}}.$$

where I_{EFF}, $J_1(m)$, etc. are the same as defined before. This expression together with the shot noise formula in chapter 4.1 show that I_{DET} should be small enough as compared with I_{DC} in order to make the electrical noise negligible for the shot noise. We have measured the I_{DET} using an incandescent lamp and obtained a rather small value, 0.08 mA. Since the typical value of I_{DC} in our interferometer is 0.52 mA, the electrical noise in the main feedback loop is smaller than the current shot noise level.

The modulation circuit may also produce electrical noise by applying voltages to the Pockels cell directly. We verified that this noise was much smaller than the current shot noise.

Another important noise comes from the local control system. In principle, the mirrors should be controlled locally only around the resonance frequency of the pendulum; in the interested frequency range, the mirrors must act as free masses. For this purpose, feedback signal is rolled off rapidly above approximately 10 Hz. The amplifier in the final stage is, however, left wide-band to allow the use of the coil-magnet system for the interferometer locking. Thus the electrical noise in the final stage cannot be eliminated by filtering. This noise results in a path difference change of 4×10^{-16} m/$\sqrt{\text{Hz}}$ at 1 kHz.

5. Frequency Stabilization

5.1 Necessity of Frequency Stabilization

The measurement of a differential length change in a Michelson interferometer puts relatively little demand on the frequency stability of the illuminating laser light. This is because this type of interferometers with equal path lengths are inherently insensitive to changes to the wavelength of the light. In reality the degree of frequency stability required is still rather high, because of the difficulty in achieving equal path lengths and the presence of scattered light.

In the delay line scheme, with the presence of the curvature differences between the delay-line mirrors, the re-entrance condition is not compatible with equal path length in the two arms. This practical problem imposes a high degree of stabilization on the laser frequency.

In addition, the scattered light may produce considerably large noise in combination with laser frequency fluctuation. Even if the delay-line mirrors are made with exactly the same curvature, the scattered light will have a large path difference to the main beam. Therefore frequency stabilization is absolutely necessary for this system.

5.2 RF Reflection Locking

There has been a great deal of work done on the development of short-term frequency stabilization techniques. One of the passive methods is to isolate the laser

cavity from the vibrations introduced by the cooling water. Although we did not adopt this method, we found that the frequency fluctuation could be reduced considerably by reducing the cooling water flow.

Any active method of stabilization requires a frequency reference discriminator with high short-term stability, where a Fabry-Perot cavity is often used. Similar to the case of the main interferometer, there are mainly two methods for the frequency stabilization system using a Fabry-Perot cavity as a discriminator: the differential method and the rf reflection locking technique.

In the differential method, the transmitted light from the cavity is compared with a sampled beam and the differential signal is fed back to the laser. This comparison is necessary to eliminate the conversion of laser intensity fluctuations into apparent frequency noise. On the other hand, the rf reflection locking technique uses radio-frequency modulation to make the system insensitive to the intensity fluctuations.

We tried both methods and found the latter is preferable to the former in terms of attained stabilization. The reason is as follows. The differential method is subject to mechanical vibration of the system as well as changes of beam directions. This is because such perturbations change only the transmitted light from the cavity but not the reference beam and then cause mimic deviation signals. On the other hand, the method of the rf reflection locking, where the laser frequency is locked to the resonance peak of the cavity, has only a small dependence on such fluctuations; because the resonance frequency does not move to first order, even if the intensity at the resonance peak is changed by mechanical vibrations or beam jitter.

A schematic diagram of the frequency stabilization system using the rf reflection locking technique is shown in Fig. 5.2.1. A small fraction (approximately 5%) of the laser light before injection to the optical fiber is sampled and phase modulated by passage through Pockels cell (621–042; Inrad) at 11.5 MHz. The modulated light, which is linearly polarized, passes through a polarizing beamsplitter and a quarter-wave plate. The axes of the quarter-wave plate are oriented at $\pm 45°$ to the polarization of the input light. As a result, the resulting light becomes circularly polarized. This light enters a Fabry-Perot cavity, which has a length of 25 cm and a finesse of 300. The light coming back from the cavity, which is also circularly polarized, is then transformed to linearly polarized light by the quarter-wave plate with a polarization orthogonal to that of the incident light. Consequently this light is all reflected by the polarised beamsplitter and is detected by a photodetector (PIN photodiode).

This reflected light from the cavity has two components: one is the light reflected directly from the input cavity mirror and the other is the light which leaks back out of the cavity. The directly-reflected light is still phase modulated like the input light; the amplitude A_0 for a small modulation index m has the form of

$$A_0 = a_0 \{J_0(m)\sin \omega t + J_1(m)\sin(\omega+\omega_m)t - J_1(m)\sin(\omega-\omega_m)t\} ,$$

where ω is the angular frequency of the laser light, ω_m is the modulation angular

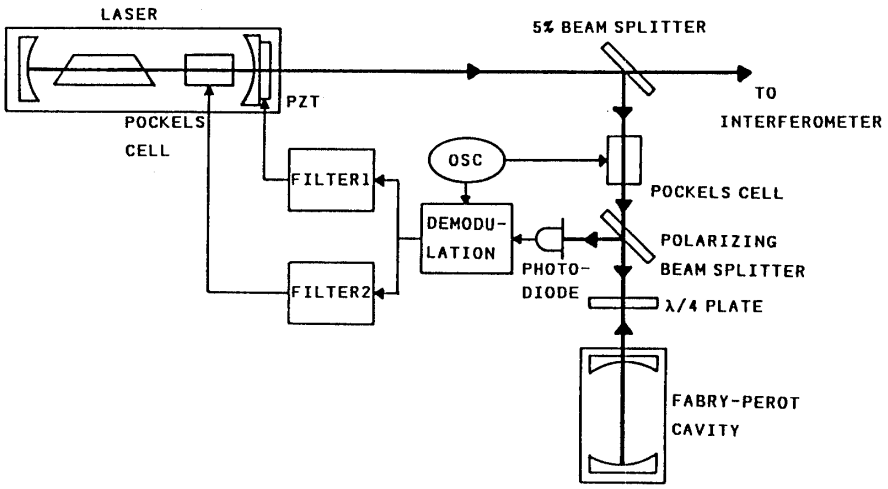

Fig. 5.2.1 Schematic diagram of the frequency stabilization system using the rf-reflection-locking technique. The Fabry-Perot cavity is used as the frequency reference discriminator. The intracavity Pockels cell and the PZT attached to the laser cavity are used to control the laser frequency.

frequency, and J_0 and J_1 are the zeroth and the first order Bessel functions, respectively. On the other hand, the light emerging from within the cavity has no more sideband frequencies, because the sidebands lie outside the resonant line width of the cavity (about 1 MHz); this light has amplitude A_c given by

$$A_c = a_c\ J_0(m)\sin(\omega t+\Phi),$$

where Φ is a measure of the relative phase between the input light and the light in the cavity. As a result, the intensity of the total reflected light, or in other words, the interference light between the two components detected on a photodiode, has a component at the modulation frequency $P_{\omega m}$ proportional to Φ which in turn is (to first order) proportional to the deviation of the light frequency from the resonance peak:

$$P_{\omega m} = a_0\ a_c\ J_0(m)\ J_1(m)\Phi.$$

If the laser light is precisely in resonance with the cavity, the photodiode output has no component at the modulation frequency.

The output of the photodiode is demodulated to get the deviation signal from the resonance peak. The deviation signal is filtered, amplified and fed back to the laser to lock the laser in wavelength to the Fabry-Perot cavity in two ways: by a piezoelectric transducer attached to the fore mirror of the laser and by a Pockels cell inside the laser cavity. The low frequency part, with its large dynamic swing, is handled by applying the feedback signals to the piezoelectric transducer, while the high frequency part is applied to the intracavity Pockels cell, which has an inherently fast response.

The aim of the laser stabilizing system for detecting gravitational wave is to achieve

the requird level of frequency stability for the laser in the interesting frequency range around 1kHz. Thus we need high open loop gain around 1 kHz. For this purpose, the slope of the open loop gain is 20 dB/decade around the unity gain frequency, which is at 300 kHz in our case, and is increased to 40 dB/decade at lower frequencies. Figure 5.2.2 shows the open loop gain of the feedback system: the loop gain at 1 kHz is 80 dB and the crossover frequency between the two paths is 100 Hz.

The modulation frequency used here should be separated from that of the main interferometer by at least 1 MHz. This is because we wish to ensure that there will be no interaction between the two feedback systems.

5.3 Noise in Frequency Stabilization System

A fundamental limit to the fluctuation in frequency in this scheme is the shot noise in the detected light. The linear spectral density of the frequency fluctuation for the shot noise is given by

$$\delta\nu = \Delta\nu_c \sqrt{\hbar\omega / P_0 T\eta},$$

where $\Delta\nu_c$ is the reference cavity bandwidth (full width at half maximum), P_0 the mode-matched input laser power, T the transmission efficiency of the cavity on resonance, and η the quantum efficiency of the photodiode.

In the actual set-up, this limit is deteriorated due to the imperfect visibility in reflection of the cavity fringes and the imperfect mode matching. The actual limitation

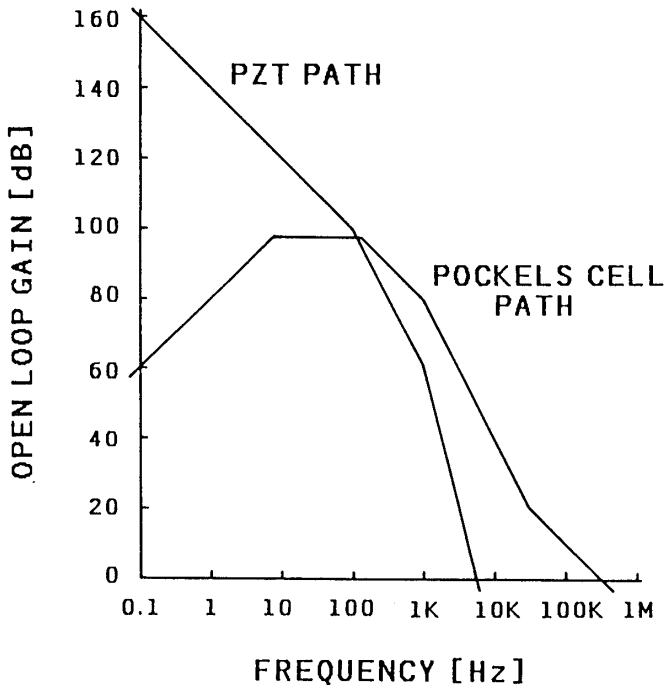

Fig. 5.2.2 Schematic view of the open loop gain in the frequency stabilization system. The PZT path and the Pockels cell path are indicated.

depends on the apparent visibility V in reflection of the cavity fringes without any modulation, which is defined by

$$V=\frac{P_{max}-P_{min}}{P_{max}},$$

where P_{max} and P_{min} are the light power in the reflected light at the maximum and minimum, respectively. From the values we have: $V\simeq 0.16$, $m=0.18$, and $P_{max}=10$ mW, the shot noise can be calculated [*18*] [*19*] and is,

$$\delta v=0.05\ \mathrm{Hz}/\sqrt{\mathrm{Hz}}.$$

Another possible noise source is mechanical vibrations. The rf reflection locking system is, to first order (only if perfectly confocal), insensitive to beam jitter relative to the Fabry-Perot cavity, which is caused by movement of the laser beam itself or vibrations of the optical components used for the system. More critical is the vibration of the cavity length. To suppress it, we set the cavity on two sets of metal plates and rubber and put them in the vacuum.

6. Performance of the 10 m Interferometer

6.1 Local Control

The local control system worked very well, although the relatively small dynamic range of the sensor (Fig. 6.1.1) demands a precise adjustment in setting the local control unit. Figure 6.1.2 shows the response of the mirror motion to an impulsive force with the local control system at different gains. The force was exerted to the mirror by applying an electrical pulse to the coil of the local control system. In the case

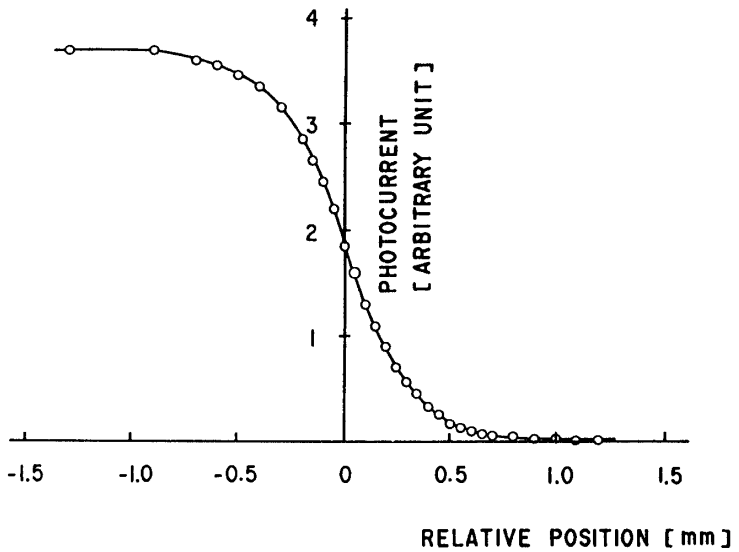

Fig. 6.1.1 Measured photocurrent of the photodiode used for the local control sensor as a function of the relative position of the sensor and the mirror.

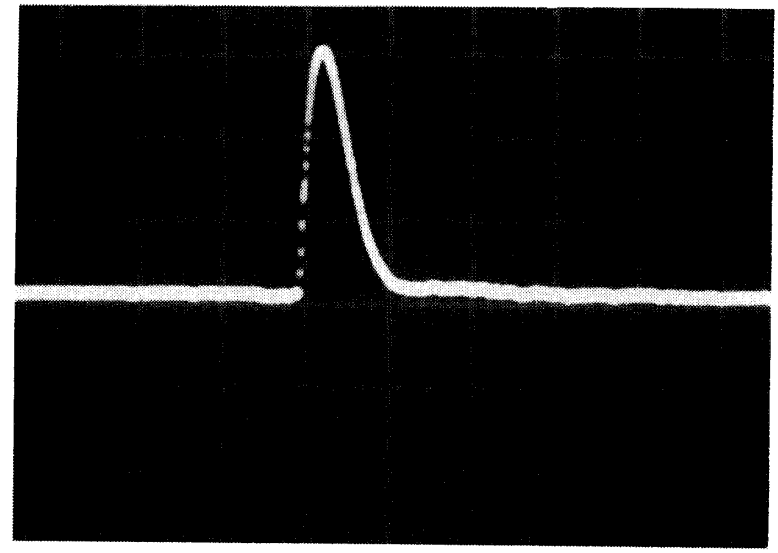

(a)

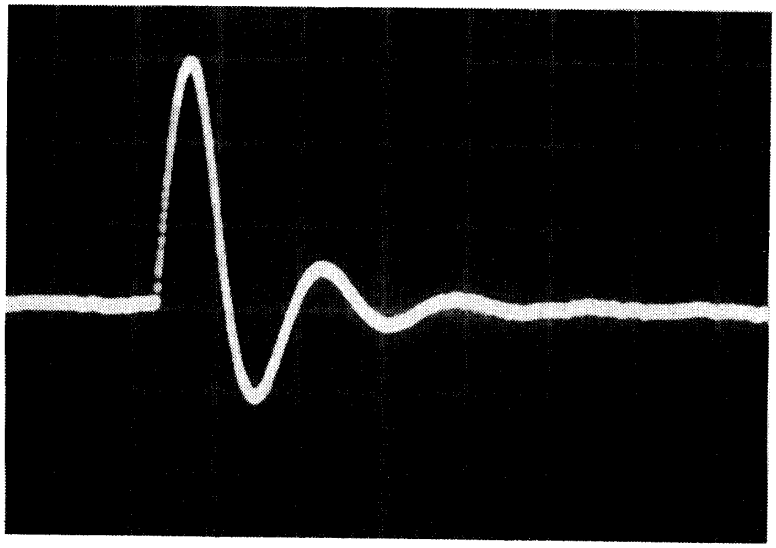

(b)

Fig. 6.1.2 Response of the mirror motion to an impulsive force with the local control system at different gains. (a) The mirror motion is damped completely (critical damping); and (b) with a smaller gain, the mirror is damped after a few oscillations.

of critical damping, the mirror motion is damped without any rebound (a). With a smaller open loop gain of the feedback system, the mirror is damped after a few oscillations (b).

6.2 Frequency Stabilization

The transmitted laser intensity, the reflected laser intensity, and the demodulated signal, as the resonant frequency of the cavity is scanned, are shown in Fig. 6.2.1. In the figure of the transmitted intensity, two clear sidebands can be seen. The figure of the demodulated signal illustrates that the signal is proportional to the frequency

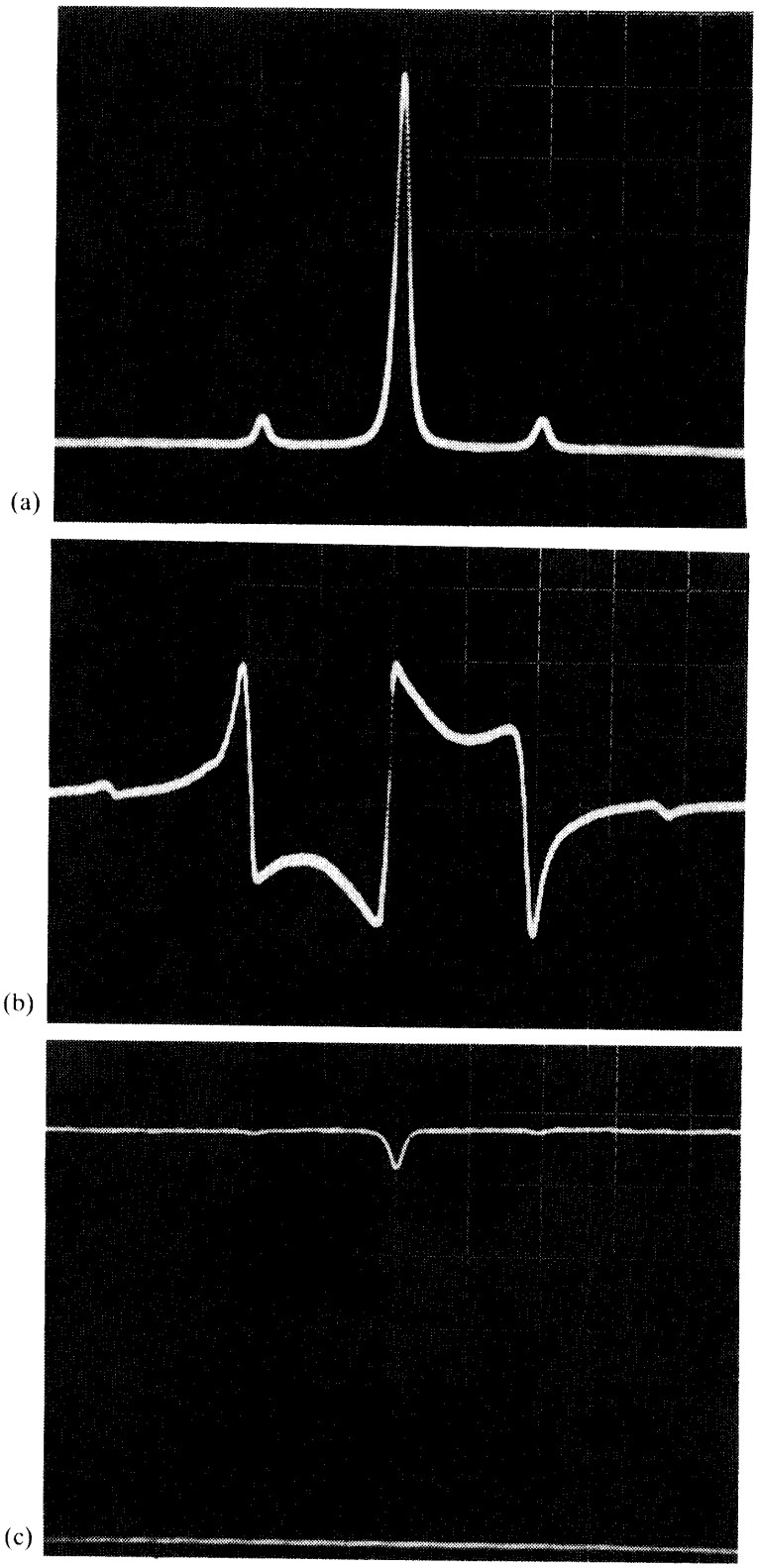

Fig. 6.2.1 (a) Transmitted laser intensity; (b) the demodulated signal; and (c) the reflected light, as the resonant frequency of the Fabry-Perot cavity is scanned.

deviation from the resonance point around the resonance.

Figure 6.2.2 shows the improvement in the frequency stability. The upper curve is the linear spectral density of the frequency fluctuation of the unstabilized laser. This is the correction signal applied to the Pockels cell in the laser. The lower curve is the error signal (after demodulation) in the laser stabilizing loop expressed in terms of equivalent fluctuations in the laser frequency. This level of stabilization can only be attained if the Fabry-Perot cavity and the other optical components involved have sufficient mechanical stability. The stabilized frequency flucturation is 0.3 Hz/$\sqrt{\text{Hz}}$ at 1 kHz, which is about a factor of six above the shot noise of the system.

6.3 Attained Sensitivity

In the interferometer, the deviation signal from a certain dark fringe is fed back to one Pockels cell and a driver of one end mirror after appropriate amplification and filtering in order to lock the system to the operating point. We designed the feedback system so that the Pockels cell path may be dominant in the feedback loop above 100 Hz and have an unity gain frequency of 100 kHz. We also verified that the Pockels cell has no resonance in terms of the phase modulation effect below 100 kHz. As a result, we can consider the amplitude of the feedback signal to the Pockels cell to be proportional to that of the original fluctuation of the total path difference in the interferometer between 500 Hz and 20 kHz with an error of at most 0.2 dB.

The efficiency of the Pockels cell used for the feedback control in the main interferometer is 2.6×10^{-10} m/V (single passage), which is defined as the change of the effective length divided by the applied voltage. It was measured in advance with the help of the laser and a spectrum analyzer as follows. The pockels cell was inserted in the laser cavity and voltage was applied to it. The variation in the laser single-mode

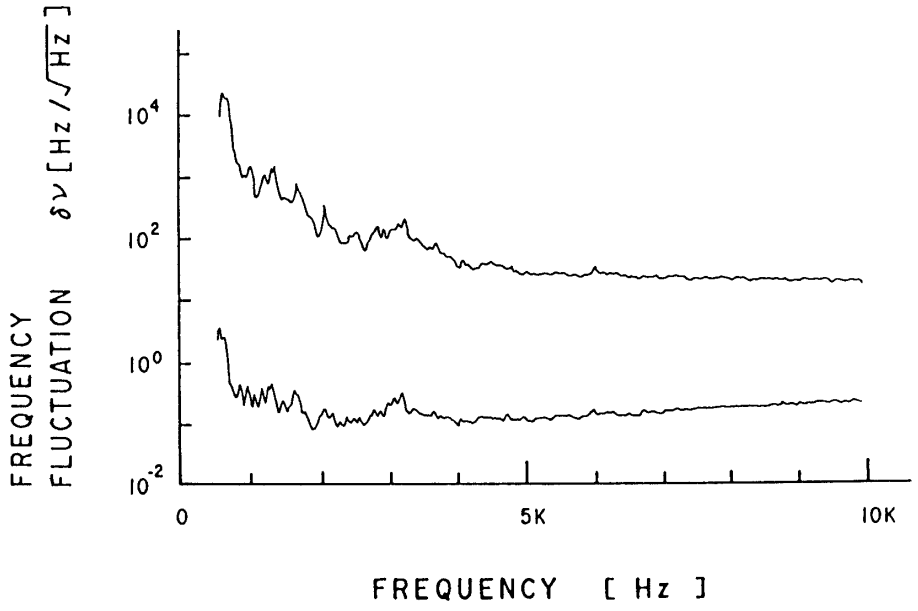

Fig. 6.2.2 Natural frequency fluctuation of the Ar^+ laser used (upper curve), and the error signal in the frequency stabilizing loop (lower curve) expressed in terms of equivalent frequency fluctuation.

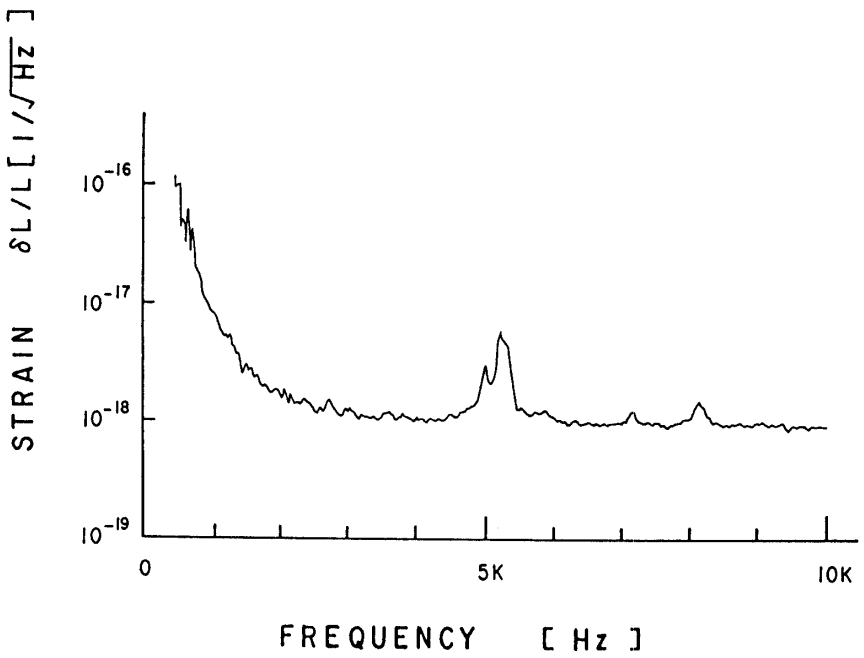

Fig. 6.3.1 Noise spectrum of the 10 m prototype for the laser interferometer gravitational wave antenna in terms of the linear spectral density of the gravitational wave strain.

frequency due to the applied voltages was measured with a light spectrum analyzer.

Figure 6.3.1 shows the typical noise spectrum of the 10 meter interferometer with 102 reflections and an effective light power of 30 mW. The vertical scale is the logarithm of the strain $\delta L/L$, provided the observed noise be completely attributed to the strain. This noise spectrum was obtained by analyzing the feedback signal at the Pockels cell of the interferometer with a Fourier transform spectrum analyzer (T592A, Advantest). It was operated with a frame time of 40 msec and 128 averages.

In the frequency range below 1 kHz, a very high noise level can be seen. From 1 kHz to 3 kHz the noise slowly decreases with increasing frequency. The noise level of $1.6\times10^{-18}/\sqrt{\text{Hz}}$ is achieved at 2 kHz. At 5.2 kHz, a relatively broad peak can be seen. Above 6 kHz the noise spectrum is flat except for a few small peaks. The noise value of this floor is $9.5\times10^{-19}/\sqrt{\text{Hz}}$ for the strain.

6.4 Noise Behavior

(i) Shot Noise

The calculated shot noise is $8.5\times10^{-19}/\sqrt{\text{Hz}}$ for the values used: the maximum photocurrent $I_{MAX}=8.8$ mA, the interference contrast $K=0.92$, and the modulation index $m=0.44$. This value is close to the present noise floor above 6 kHz.

(ii) Laser Intensity Noise

Figure 6.4.1 shows the intensity fluctuation of the Ar^+ laser used for our interferometers. The intensity fluctuation $\delta I/I$ is about $10^{-4}/\sqrt{\text{Hz}}$ around 1 kHz. On the other hand, the ground noise driven fluctuation in the difference between the total path lengths is at most 50 μm around 1 Hz in the case of 102 reflections in the delay

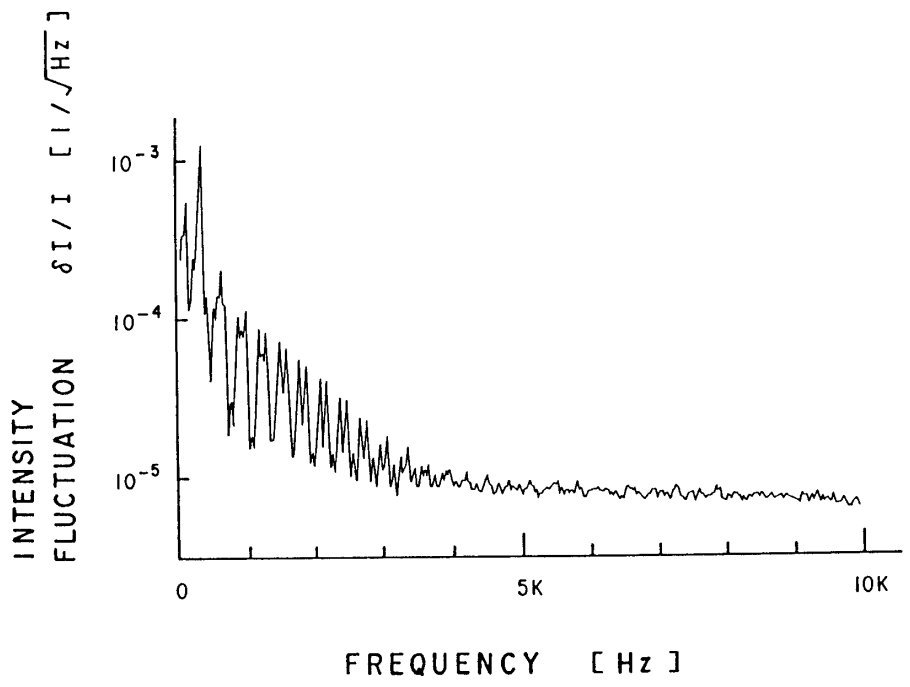

Fig. 6.4.1 Intensity fluctuation of the Ar^+ laser used.

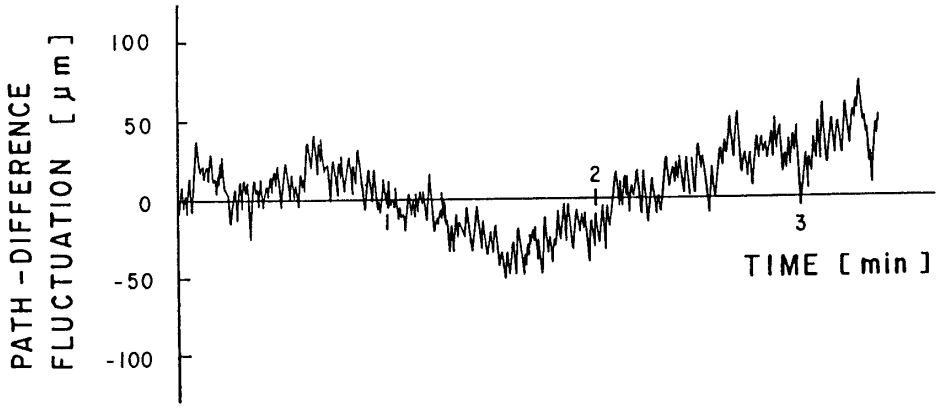

Fig. 6.4.2 Path difference fluctuation between the two arms.

line (Fig. 6.4.2). And the open loop gain of our feedback system at 0.5 Hz reaches a relatively high value of about 10^9. Therefore, we can suppress the intensity noise δL_{IN} to the equivalent displacement level of 2×10^{-18} m/$\sqrt{\text{Hz}}$ around 1 kHz only by locking the light to dark fringes. This is low enough as compared with the present noise level.

Figure 6.4.3 shows the interferometer noise spectrum with an operating point deviating a little from a dark fringe. The deviation was caused by applying an offset voltage at the initial stage of the main feedback amplifier. The resulting noise spectrum has almost the same shape as the original intensity fluctuations (Fig. 6.4.1), except for some resonance peaks. It was also proved that the intensity noise can be suppressed below the current noise level of our interferometer only by locking the

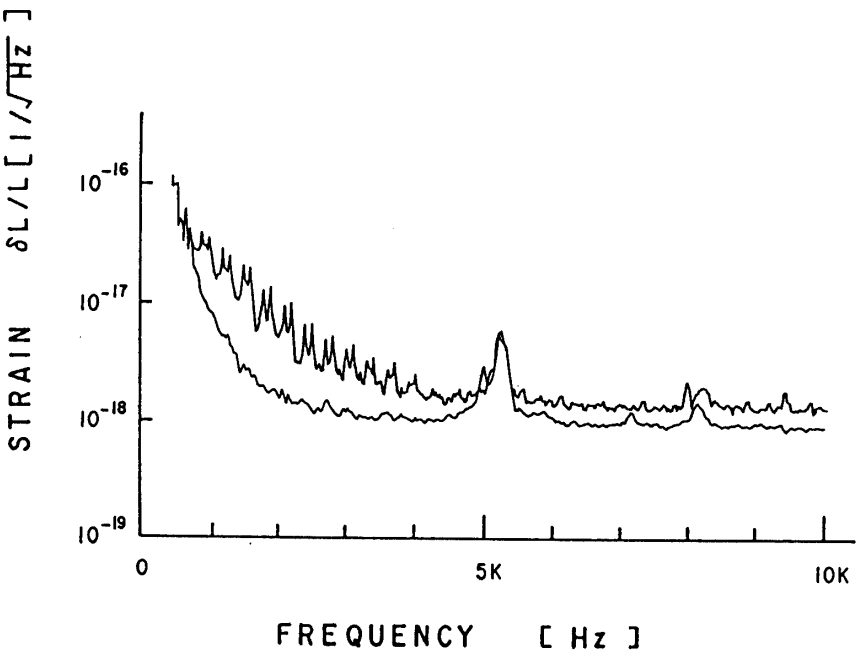

Fig. 6.4.3 Interferometer noise spectrum with (upper trace) and without (lower trace) an artificial offset of the operating point from the dark fringe.

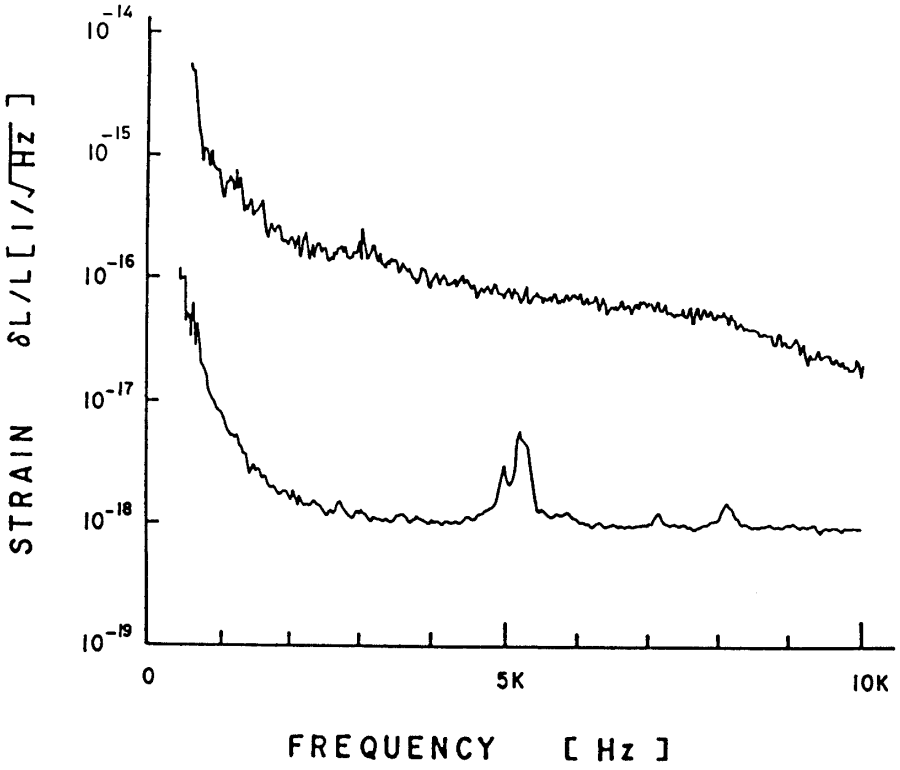

Fig. 6.4.4 Interferometer noise spectrum with (lower trace) and without (upper trace) frequency stabilization of the laser.

system precisely to the minimum of intensity at the interferometer output.

(iii) Laser Frequency Noise

Figure 6.4.4 shows the noise spectrum with and without the frequency stabilization system. It is clear that the noise with the unstabilized laser is totally due to the laser frequency fluctuations. We can also see from this figure that a considerable amount of frequency stabilization has actually been realized.

(iv) Laser Beam Geometrical Noise

The noise due to the laser beam jitter can be easily suppressed by adjusting the angle of the beamsplitter. An artificial beam jitter noise produced by vibrating the fiber end block with the magnet-coil system of the local control can be used to help in the alignment. The beamsplitter should be adjusted so that the artificial noise is minimized.

(v) Scattered Light Noise

In order to artificially produce up-conversion noise, one of the end mirrors was moved at a constant speed of about 9 μm/sec with the help of the local control system. As a result, a series of peaks appeared in the noise spectrum of the interferometer as shown in Fig. 6.4.5. The frequencies of the peaks, which are multiples of a basic mode, were found to be due to the scattered light with multiples of a full round trip. The peak just below 2 kHz is the up-conversion noise of the scattered light with one

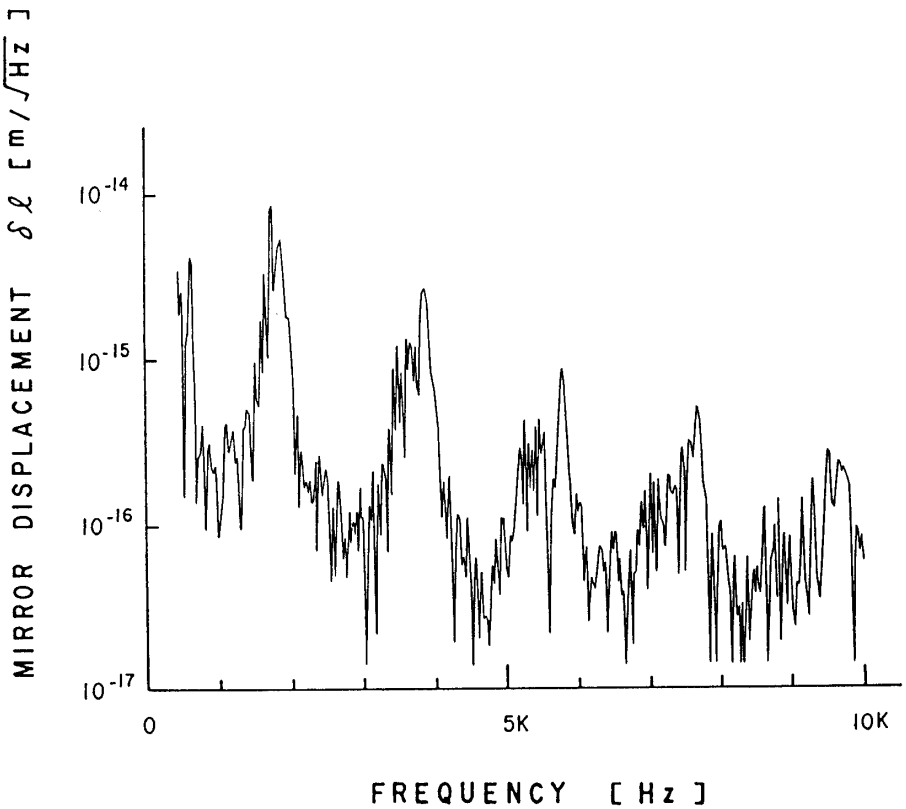

Fig. 6.4.5 Interferometer noise spectrum with the artificial up-conversion noise of the scattered light. The artificial noise was obtained by moving the end mirror at a constant speed.

additional full round trip in the delay line.

The amplitude of each scattered light noise can be estimated roughly from the figure. The results are as follows:

(1) the amplitude of the dominant scattered light with one additional full round trip in the delay line is approximately 10^{-4}.

(2) the amplitude of the scattered light with N additional full round trips seems to be approximately $(1/3)^{N-1}\times10^{-4}$.

These results accord considerably well with the values reported by Schilling and his collaborators [*20*].

Since the path length of our interferometer is fluctuating with a variation of 50 to 100 μm/sec owing to the pendulum motion, the noise caused by the scattered light with 10 to 5 additional full round trips may appear around 1 kHz in the noise spectrum of the interferometer. These noise should be 5×10^{-17} to 1×10^{-14} m/$\sqrt{\text{Hz}}$ in terms of path difference, according to the amplitude of the scattered light obtained above. Therefore, the present noise level around 1 kHz can be explained by the up-conversion of the scattered light. The easiest way to reduce the up-conversion noise is to install black rings around the holes in the near mirrors. We tried this method and found that such black rings reduced the up-conversion noise around 1 kHz by about 5 dB.

(vi) Seismic Noise

Although we have neither a sensitive accelerometer nor a powerful vibrator, we set an upper limit of the seismic noise as 4×10^{-17} m/$\sqrt{\text{Hz}}$ at 1 kHz. This was determined by vibrating the system and monitoring the acceleration of it and the corresponding noise in the interferometer output.

(vii) Thermal Noise

At 5.2 kHz a broad peak is visible. This peak consists of four steep peaks with a bandwidth of about 1 Hz and one relatively broad peak (Fig. 6.4.6). The narrow peaks are probably due to the resonances of the mirrors, because the calculated frequency agrees quite well with the measured value. The broad peak has not yet been identified.

(viii) Gas Pressure Noise

Figure 6.4.7 shows the build-up of the vacuum system pressure. It takes about 8 hours for the vacuum to come up to 10^{-4} mbar. We evacuated the system before each operation, which ensured a negligible level of the gas pressure noise in each measurement.

(ix) Electrical Noise

The electrical noise of the O/E preamplifier in this case is calculated to be $3.2\times10^{-19}/\sqrt{\text{Hz}}$ from the measured value of I_{DET} of 0.08 mA. In addition, artificial electrical noise was produced by applying 10^2 times the O/E preamplifier noise to the electrical circuit for the feedback control (Fig. 6.4.8). The resulting electrical noise was $2.6\times10^{-17}/\sqrt{\text{Hz}}$, which is in good agreement with the calculated value.

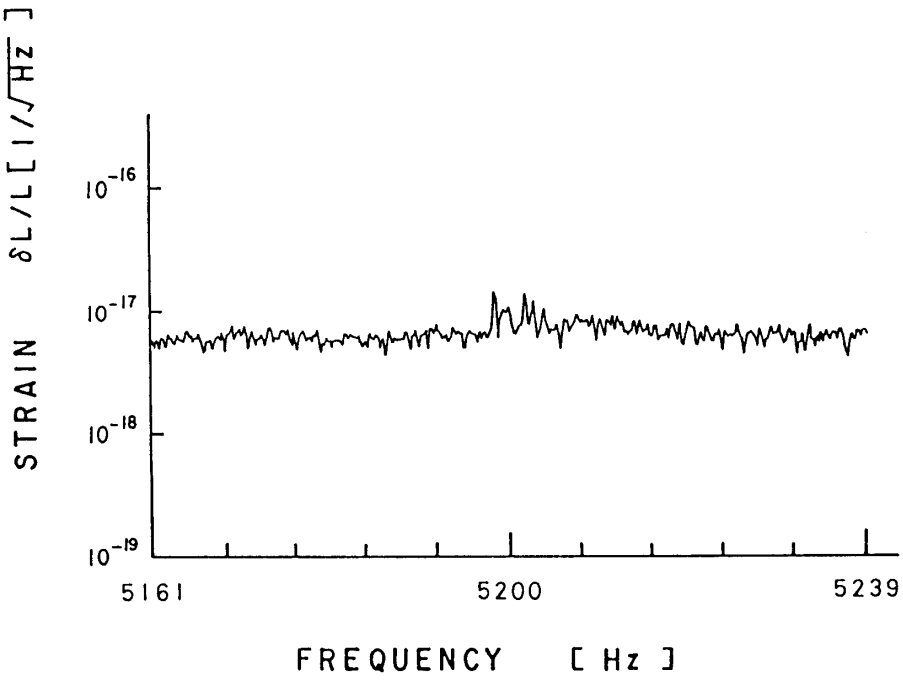

Fig. 6.4.6 Resonance Peak of the mirrors at 5.2 kHz in the interferometer noise spectrum.

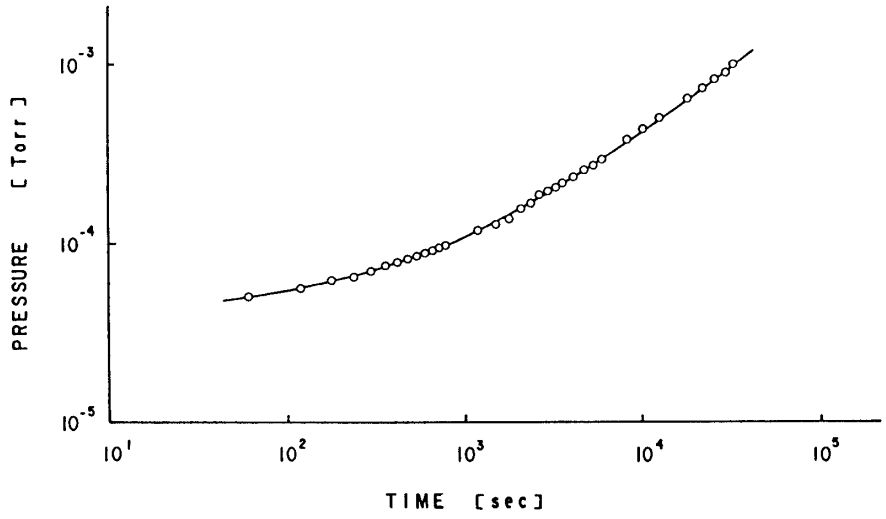

Fig. 6.4.7 Build-up of the vacuum system pressure of the interferometer. The initial vacuum is 3×10^{-5} mbar.

7. Long Data Taking Runs

7.1 Data Acquisition System

Although we had recognized the importance of the extended data taking, the direct motivation for this long-term operation was the discovery of a possible pulsar in the remnant of the supernova 1987A. Shortly after the discovery, we started to operate our interferometer antenna. This was the first time that our interferometer was

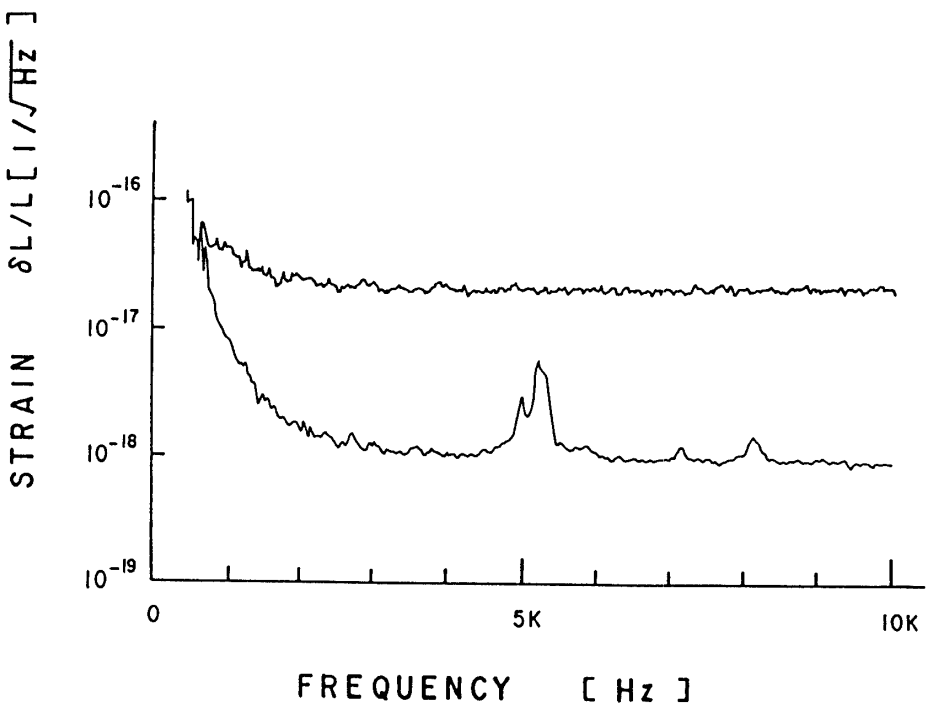

Fig. 6.4.8 Interferometer noise spectrum with the artificial electrical noise. The applied electrical noise is 10^2 larger than the natural electrical noise of the O/E preamplifier.

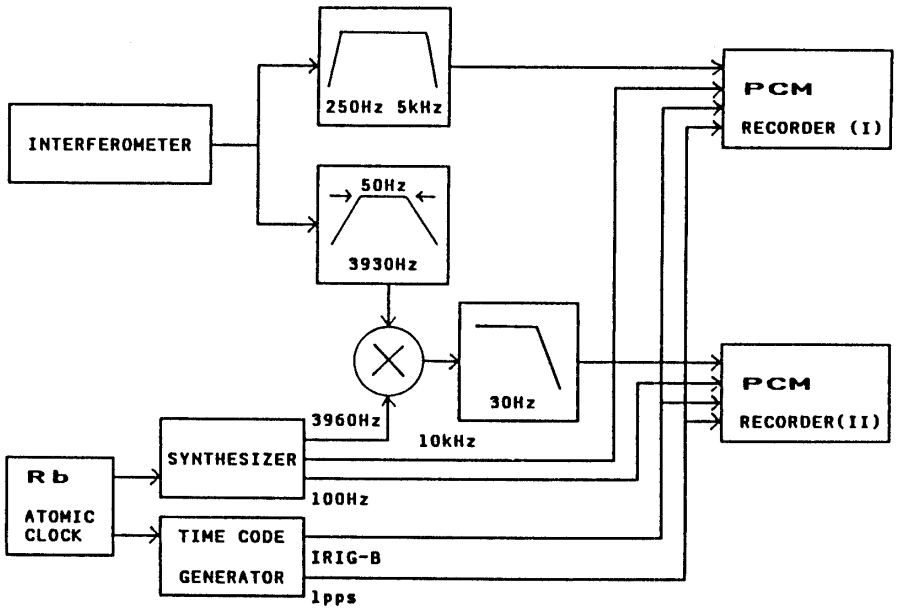

Fig. 7.1.1 Data acquisition system (I). The wide band data and the down-converted 4 kHz data are recorded by the PCM video recorders together with the time code and the reference clock.

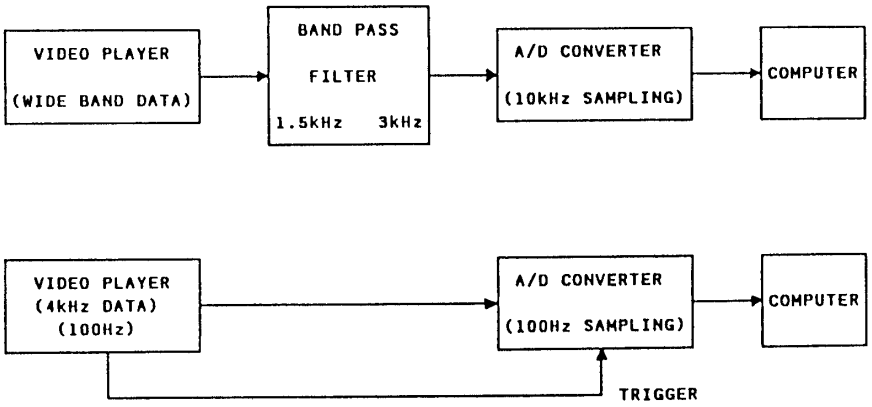

Fig. 7.1.2 Data acquisition system (II). The wideband data are filtered again and, through the A/D converter, stored in the computer. The 4 kHz data series is A/D converted with its own clock and saved.

operated for such a long period.

The data acquisition system including the narrow band data channel for pulsar search is shown in Fig. 7.1.1 and Fig. 7.1.2. In the noise spectrum of our interferometer (Fig. 6.3.1), we can see the steep rise towards low frequencies, from about 1 kHz downward. Because of the limited dynamic range of the A/D converter, the large noise contributions at low frequencies cannot be tolerated. For this reason we cut off the lower frequency range below 250 Hz.

As for the high frequency side, we should retain as much of the noise information as possible. Since we chose an appropriate sampling rate of 10 kHz, we cut off the data above the Nyquist frequency 5 kHz, given by half the sampling rate. We should prevent spurious contributions from higher frequencies. For this purpose we used filtering with -80 dB/decade roll off starting from the Nyquist frequency 5 kHz on upwards.

The wide band data was recorded directly after the filtering by the PCM video recorder I (see Fig. 7.1.1). As for the narrow band data, the output of the interferometer was multiplied by a 4 kHz signal and low-pass-filtered. As a result, the output signal was down-converted to very low frequencies. It was also recorded by the PCM recorder II. Time code (IRIG-B) and some reference signals (10 kHz, 100 Hz, and 1 puls per second) were also recorded. The video recorders allow storage of up to 6 hours of data on one small cartridge.

For February 20 to March 12, we used the data acquisition system to take data for several hours almost every night. We recorded on the video tapes a total of 126 hours of data over a period of 21 days (ref. Table 7.1.1).

After the data taking, part of the data were stored into a computer. The wide band data were filtered again (Fig. 7.1.3) in order to pick up a limited frequency range between 1.5 kHz and 3 kHz, and were input through the A/D converter. The narrow band data series was stored in the computer directly with its own time reference.

Table 7.1.1 Operation record of the long data taking run performed 2.20-3.12 using the 10 m laser interferometer.

DATE 1989	PERIOD (WHOLE OPERATION)	PERIOD ($h<2\times10^{-18}/\sqrt{Hz}$) #
2.20	2:00-10:00	
2.21	1:30- 8:00	
2.23	3:00-13:00	
2.24-2.25	23:30-11:00	
2.25-2.26	23:40- 8:45	4:00- 8:10
2.27	1:10- 7:20	1:10- 4:50
3. 1	1:10- 6:30	
3. 2	3.35- 7:30	3:25-7:30
3. 3	0:20- 7:30	0:27- 5:30
3. 4	0:30- 6:25	0:30- 6:25
3. 6	2:25- 8:20	
3. 6-3. 7	23:40- 6:30	1:20- 6:30
3. 7-3. 8	23:45- 4:20	23:45- 2:30
3. 9	0:20- 6:25	
3.10	0:20- 7:35	0:20- 4:35
3.10-3.11	23:00- 4:50	23:00- 4:50
3.11-3.12	21:45-13:50	21:45-23:10
		3:10- 4:00
		5:15- 6:30
		11:35-13:50
TOTAL TIME	126 hours	46 hours

at 4 kHz

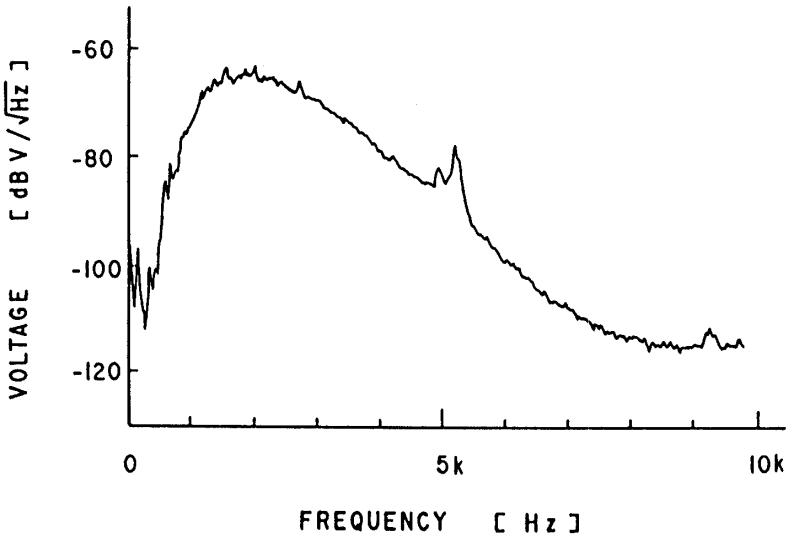

Fig. 7.1.3 Resultant noise spectrum of the wideband signal which is stored in the computer.

7.2 Long-term Stability

The 10 m prototype was operated for more than 5 hours continuously, whereas the longest continuous run of laser interferometer antennas ever made without any interruption had been only 1–2 hours.

Success of this continuous operation was mainly attributed to the optimal design of the feedback control system used. Two important feedback systems, the main feedback and the frequency stabilization system, are very complicated and conditionally stable. In addition, the dynamic ranges of each are relatively small. Therefore, unlocking of the feedback system can easily occur. We designed the system carefully so that the breakdown rarely occurs.

Laser mode jumps, which had been reported by the Max Planck Institute as a principal cause for the breakdown of the system, have been avoided by compensating for the thermal change in length of the Fabry-Perot cavity for the frequency stabilization system. Although the compensation system was manual, it worked well.

The laser mode instability was found to be the major cause for the unlocking of the frequency stabilization system. We verified that after most breakdowns in the frequency stabilization system, an additional mode in the laser had appeared. It was found to occur either spontaneously or because of the light returning to the laser from the fiber surface.

The spontaneous mode instability seems to be due to the intracavity Pockels cell, because without the Pockels cell inside the laser, no mode instability was found. Although it may be possible to avoid the mode instability even with the Pockels cell in the laser, the more desirable method is to remove the Pockels cell. Whereas the frequency stabilization system will be much more complicated without the intracavity Pockels cell, no power loss due to it would permit the substantial reduction of shot noise.

The mode instability due to the light returning to the laser is understandable, since there is no optical isolator before the fiber. This will be easily svoided by using an isolator.

The noise level of the system deteriorated with the passage of time. It was found to be due to a deterioration of the interference contrast, which may be caused by any change in the mirror angle or position. The noise level was easily restored by adjusting the contrast again. Fortunately it is possible to adjust without turning off the feedback system.

Another problem for the data taking originates from the noise environment of our interferometer. It is not situated in a separate room but shares the room with several other large experiments. The great deal of activity near the interferometer does not permit its operation in the daytime. Hence data taking must be performed between midnight and early morning.

7.3 Noise Distribution

Figure 7.3.1 shows the typical noise distribution of the interferometer for 1 hour with a frequency range from 1.5 kHz to 3 kHz. The large deviation from the Gaussian

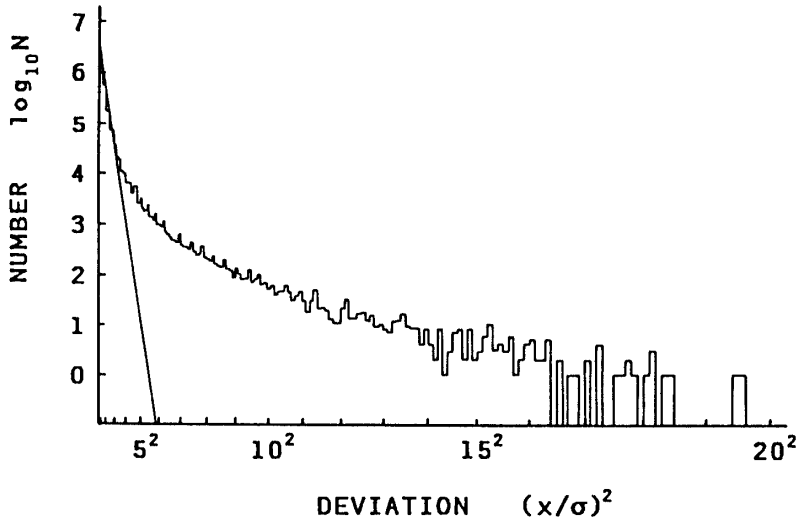

Fig. 7.3.1 Typical noise distribution of the wideband data calculated from 1 hour of data. The solid line indicates the gaussian distribution.

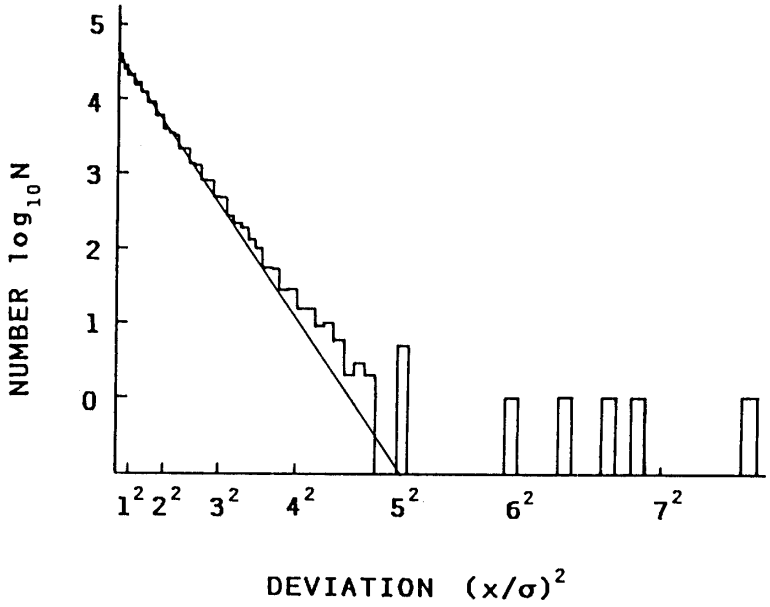

Fig. 7.3.2 Typical noise distribution of the 4 kHz narrow band data calculated from 3 hour of data. The solid line indicates the gaussian distribution.

distribution indicates that the dominant noise in this frequency range is not stationary but fluctuating up and down at relatively low frequencies. This is consistent with the result in chapter 6 that the up-conversion noise of the scattered light noise is dominant in this frequency range.

On the other hand, Fig. 7.3.2 shows the noise distribution around 4 kHz with a bandwidth of 30 Hz for 3 hours of data. This distribution is much closer to the Gaussian distribution. It indicates that the up-conversion noise is relatively small

around 4 kHz. Five burst-like events out of 10^6 data points were detected in the 3 hour period. We also analyzed the wide band data corresponding to that period. However, we could not attribute the 5 bursts to up-conversion noise. Although their origin could not be found, 5 unidentified events out of 10^6 points is infrequent enough to be removed by taking the correlation between two antennas operating at the same time.

8. Conclusion

For the 10 m prototype of a laser interferometer gravitational wave antenna a sensitivity level sufficient for further development of a larger antenna has been achieved by successfully suppressing the various noise sources. In the frequency range above 3 kHz, the sensitivity was practically limited by the theoretical shot noise. Below 1 kHz, however, the noise level is still fairly large as compared with the current shot noise level. The excess noise was found mainly to be due to the up-conversion noise of the scattered light between 1 kHz and 3 kHz, and due to seismic noise below 1 kHz. The obtained sensitivity for the gravitational amplitude h was $1.6\times10^{-18}/\sqrt{\text{Hz}}$ at 2 kHz and the noise floor above 6 kHz was $9.5\times10^{-19}/\sqrt{\text{Hz}}$. Although this prototype has a total path length of only 1 km, these satisfactory results encourage us toward the development of a future larger antenna.

The 10 m prototype was operated for more than 100 hours over a period of 21 days to investigate the long-term stability and noise statistics. The data acquisition system worked very well and was found to be free of problems. The prototype was operated for more than 5 hours continuously, whereas the longest continuous run of laser interferometer antennas ever done had been only 1–2 hours.

Success of this continuous operaion was mainly attributed to the optimal design of the feedback control system used. In addition, laser mode jumps, which had been reported by the Max Planck Institute as a principal cause for the breakdown of the system, has been avoided by compensating for the thermal change in length of the Fabry-Perot cavity for the frequency stabilization system. The laser mode instability was found to be the major cause for the unlocking of the frequency stabilization system.

Large burst-like signals which have an amplitude well above the level expected from the Gaussian distribution of the shot noise have been detected and analyzed. Only 5 unidentified bursts out of 10^6 data points were detected around 4 kHz with a bandwidth of 30 Hz. Spurious signals with such infrequency can be easily eliminated by taking correlation between two antennas operating simultaneously.

In future larger interferometer antennas, an increase in the light power in various ways such as recycling is considered very important for increasing the sensitivity to the level which permits the detection of gravitational waves from the Virgo cluster. Moreover, a stable operation of the large antenna for a long period is absolutely necessary, because continuous operation over months or years will be necessary to detect and observe gravitational waves. Therefore the optimal system design which ensures the long-term operational stability is required for the large antenna. Simultaneous observation with several antennas is also especially useful for the detection of gravitational-wave bursts.

References

[*1*] J. H. Taylor, J. M. Weisberg, Astrophys. J. **253** (1982) 908
[*2*] J. M. Weisberg, J. H. Taylor, Phys. Rev. Lett. **52** (1984) 1348
[*3*] J. Weber, Phys. Rev. Lett. **22** (1969) 1320
[*4*] W. M. Fairbank, M. Bassan, E. R. Mapoles, M. S. McAshan, P. F. Michelson, B. E. Moskowitz, **MG4** (1986) 543
[*5*] H. Hirakawa, K. Tsubono and M.-K. Fujimoto, Phys. Rev. D **17** (1978) 1919
[*6*] R. Weiss, MIT Quarterly Progress Report (Research Laboratory of Electronics) **105** (1972) 54
[*7*] R. L. Forward, Phys. Rev. D **17** (1978) 379
[*8*] J. Livas, R. Benford, D. Dewey, A. Jeffries, P. Saulson, D. Shoemaker, R. Weiss, **MG4** (1986) 591
[*9*] D. Shoemaker, R. Schilling, L. Schnupp, W. Winkler, K. Maischberger, A. Rüdiger, Phys. Rev. D **38** (1988) 423
[*10*] G. P. Newton, J. Hough, G. A. Kerr, B. J. Meers, N. A. Robertson, H. Ward, J. B. Mangan, S. Hoggan, **MG4** (1986) 599
[*11*] R. Spero, **MG4** (1986) 615
[*12*] N. Kawashima, S. Kawamura, J. Hirao, Experimental Gravitational Physics eds. P. F. Michelson (1987) 332
[*13*] R. W. P. Drever, et al., Laser Spectroscopy V, Eds. A. R. W. Mckellar, T. Oka, B. P. Stoicheff, Springer Ser. Opt. Sci. **30** (1981) 33
[*14*] D. R. Herriott, H. J. Schulte, Appl. Opt. **4** (1965) 883
[*15*] R. Schilling, L. Schnupp, D. Shoemaker, W. Winkler, K. Maischberger, A. Rüdiger, MPQ **88** (1984)
[*16*] A. Rüdiger, R. Schilling, L. Schnupp, W. Winkler, H. Billing, K. Maischberger, MPQ **68** (1982)
[*17*] W. Flugge, Handbook of Engineering Mechanics, McGraw-Hill (1962)
[*18*] R. Schilling, private communication
[*19*] D. Shoemaker, A. Brillet, C. N. Man, O. Cregut, Opt. Lett. **14** (1989) 609
[*20*] R. Schilling, L. Schnupp, W. Winkler, H. Billing, K. Maischberger, A. Rüdiger, J. Phys. E **14** (1981) 65
[*21*] H. Billing, K. Maischberger, A. Rüdiger, R. Schilling, L. Schnupp, W. Winkler, J. Phys. E **12** (1979) 1043

Appendices

A. Evolution of the Laser Interferometer

First we set up a small Michelson laser interferometer to study the behavior of interferometers. This preliminary experiment used mirrors and a beamsplitter which were not suspended by wires but fixed to a table plate. The interferometer was illuminated by a He-Ne laser and had a short delay line with an arm length of 0.8 m and a reflection number of only 6. Although we could not reach a high level of performance with the interferometer, it provided us much information and experience on this extremely difficult experiment.

Encouraged by the result of the small interferometer, We proceeded to design a 10 m' prototype laser interferometer for detecting gravitational waves. After elaborate investigation of the design with experience on the small interferometer, the mechanical construction of the system was, finally, completed in 1987.

After that, we have been engaged in adjustment and improvement of the total system. Table A. 1 shows the evolution of our 10 m laser interferometer with items of each improvement and the dominant noise after each improvement. Figure A. 1 also

Table A.1 Evolution of the sensitivity in the 10 m laser interferometer antenna.

DATA	N	POWER [mW]	MAIN IMPROVEMENT	SENSITIVITY #	MAIN NOISE
87.10	4	4	DARK FRINGE LOCKING	5×10^{-16}	ELECTRICAL NOISE (MAIN FEEDBACK)
88. 4	102	1	DARK FRINGE LOCKING	3×10^{-16}	FREQUENCY NOISE
88. 5	102	1	FREQUENCY STABILIZATION (DIFFERENCE METHOD)	7×10^{-17}	ELECTRICAL NOISE (LOCAL CONTROL)
88. 6	102	1	LOCAL CONTROL EXCHANGE	5×10^{-17}	FREQUENCY NOISE
88. 7	102	10	WIRE EXTENSION FREQUENCY STABILIZATION (MODULATION METHOD) FIBER EXCHANGE	2×10^{-17}	INTENSITY NOISE ELECTRICAL NOISE (MAIN FEEDBACK)
88.12	102	40	O/E PREAMPLIFIER EXCHANGE MIRROR CLEANING	1×10^{-17}	INTENSITY NOISE
89. 3	102	40	MAIN FEEDBACK CIRCUIT	2×10^{-18}	SCATTERING (UP-CONVERSION)

Sensitivity in terms of linear spectral density of strains around 2 kHz

sketches the evolution of the sensitivity.

We started with a 4 reflection operation and, after attaining a satisfactory result, proceeded to 102 reflections. Although the sensitivity has been improved gradually, many complexities associated with 102 reflections often prevented us from identifying the remaining noise sources clearly. This was the reason that we finally decided to go back to a short interferometer without delay lines.

There are many noise effects which are, in principle, independent of the path length in the interferometer. Such effects should be identified and reduced using a rather simple interferometer with a short path length in the early stage so that we may easily analyze path-length-dependent noise in the interferometer with 102 reflections.

To this end, we modified our interferometer with delay lines to a short interferometer only by putting small mirrors at the entrance holes of the near mirrors: the arm length of the short interferometer is 0.4 m. As a result, the geometry of the light beams for the small mirrors is almost the same as that of the outgoing beam from the delay line.

Since we can bring the short interferometer to nearly perfect symmetry, the frequency stabilization system is not necessary. In addition, scattered light can be neglected, because there are no delay lines. However, the electronics used for the rf dark-fringe locking are the same as that for the 10 m interferometer except for the gain, and the Pockels cells are still used in the same manner. Accordingly we can test the system without any complexities accompanied with the delay lines.

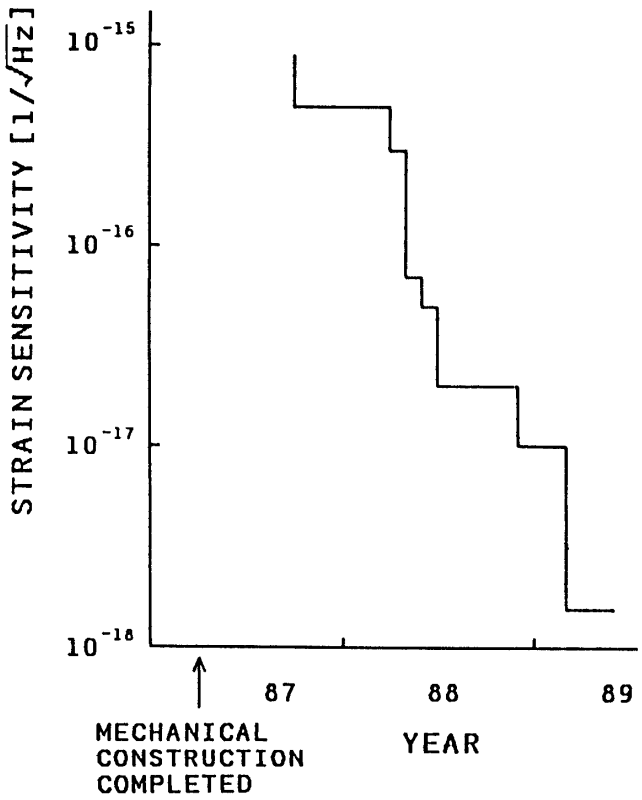

Fig. A.1 Evolution of the sensitivity in the 10 m prototype. The sensitivity is expressed by the linear spectral density of the gravitational wave strain at 2 kHz.

This experiment with the short interferometer enables us to investigate the noise with 102 reflections very easily. At present the best performance achieved is a noise level of $1.6\times10^{-18}/\sqrt{\text{Hz}}$ around 2 kHz for strains with an effective laser power of 30 mW and with 102 reflections.

B. Effect of gravitational Waves

Einstein showed in his paper on gravitational waves that a weak gravitational plane wave in an almost Minkowski space has a metric tensor given by

$$g_{ij}=\eta_{ij}+h_{ij},$$

where η_{ij} is the Minkowski metric tensor:

$$\eta_{ij}=\begin{pmatrix} 1 & 0 & 0 & 0 \\ 0 & -1 & 0 & 0 \\ 0 & 0 & -1 & 0 \\ 0 & 0 & 0 & -1 \end{pmatrix},$$

and h_{ij} is the purturbation metric tensor of the gravitational wave with all components

of the tensor much smaller than 1. If the gravitational wave propagates along the x_1 axis, h_{ij} can be represented by

$$h_{ij}= \begin{pmatrix} 0 & 0 & 0 & 0 \\ 0 & 0 & 0 & 0 \\ 0 & 0 & h_{22} & h_{23} \\ 0 & 0 & h_{32} & h_{33} \end{pmatrix} ,$$

with

$$h_{23}=h_{32},$$
$$h_{22}=-h_{33}.$$

This is a transverse wave with two polarization states.

If one assumes that the wave has components of

$$h_{23}=h_{32}=0,$$

$$h_{22}=-h_{33}=h \sin (kx_1-\omega t),$$

then the interval between two neighboring events is given by

$$ds^2=c^2dt^2- \{dx_1^2+(1+h \sin(kx_1-\omega t)dx_2^2+(1-h \sin(kx_1-\omega t))dx_3^2\} .$$

By placing free masses at various points, one can label the coordinates. The proper distance between two points is defined by the travel time of light between the masses.

If light is propagating along the x_2 axis, from $x_2=-a/2$ to $a/2$, the interval for the light is

$$ds^2=c^2dt^2- \{1+h \sin(kx_1-\omega t)\} dx_2^2=0.$$

Since $h \ll 1$,

$$c\ dt= \{1+\frac{h}{2}\sin(kx_1-\omega t)\} dx_2.$$

If the travel time of the light, Δt, is much smaller than the period of the gravitational wave, one gets

$$\Delta t= \{1-\frac{h}{2}\sin \omega t\} \frac{a}{c}.$$

One can consider the variation of Δt due to the strain in space caused by the gravitational wave. Thus the strain, $\Delta l/l$, is

$$\frac{\Delta l}{l}=\frac{h}{2}\sin\ \omega T=\frac{h_{22}}{2}.$$

For the light propagating along the x_3 axis, the strain is given by

$$\frac{\Delta l}{l}=-\frac{h}{2}\sin\ \omega T=-\frac{h_{22}}{2}.$$

C. Sources of Gravirtational Waves

There are three types of sources: bursts, continuous waves, and stochastic background. In all cases, gravitational waves are generated by relativistic motions in regions of strong gravity.

The most frequently discussed sources of gravitational wave bursts are supernovas. The collapse of stellar cores in Type II supernovas may produce millisecond bursts of gravitational waves, provided there is sufficient departure from spherical symmetry in the collapse. It is hard to predict the strength of the gravitational waves emitted from such supernovae, because of our ignorance of the initial conditions of the collapse. A supernova at the center of our galaxy would produce a strain h of the order of 10^{-18} at the earth, if the supernova released one part in a thousand of its total mass into gravitational waves. Such a strain could be barely detected by current detectors. The supernova rate in our galaxy is, however, only about 1 per 30 years. To gain a more frequent event rate, one must reach out to the Virgo cluster of galaxies. With supernovas in the Virgo cluster, we could expect strains of 10^{-21} and event rates of about 1 per month at the earth.

Another promising source is a coalescing binary star system. A close binary, which is composed of neutron stars and/or black holes, gradually spirals together because of energy loss caused by emission of gravitational waves. The quasi-periodic waves emitted by the orbit in the last 3 seconds before the collision should sweep in frequency up to kHz regions. Although this source has rather recently been recognized, the expected signal strength is quite large. Moreover, the clear and easily predicted signal from the event makes the coalescence of binaries the most reliably detectable source.

Pulsars are among the most interesting continuous wave sources to search for. The anticipated gravitational-wave strains for pulsars are much smaller. But if we know the location and period of a pulsar, we can reduce noise considerably by integrating data for a long time. Pulsars emit gravitational waves through any asymmetry about their axis of rotation; the strength of the waves depends on the size of the asymmetry. Unfortunately, it is difficult to determine such asymmetry. If we assume the ellipticity of the Crab Pulsar to be 10^{-5}, the strength of the continuous wave emitted from the Crab Pulsar will be 10^{-26} at the earth at 60 Hz.

Some cosmological processes, such as the density fluctuations that led to galaxy formation, cosmic strings, and inflation could emit gravitational waves forming a stochastic background. Since stochastic sources are randomly distributed in time and space, it is conventional to describe their energy density in the frequency range.

Experimental limits are usually quoted in terms of the universe's closure density ρ_c,

D. Optical Delay Line

Let's consider the behavior of a delay line system consisting of two equal coaxial mirrors with a radius of curvature R and a mirror distance l. A convenient coordinate system can be set so that zero point is located at the intersection between the mirrors and the axis of the delay line as shown in Fig. D. 1. In this basis, the incident beam is described by the coordinates (x_0, y_0) at the near mirror and by the slope

$$(x_0', y_0')=\left(\frac{x_1-x_0}{l}, \frac{y_1-y_0}{l}\right),$$

where (x_1, y_1) are the coordinates of the beam at the end mirror. Then one can calculate the coordinates of the n-th spots (x_n, y_n), which are given by

$$x_n=A \sin(n\theta+\alpha),$$

$$y_n=B \sin(n\theta+\beta),$$

with

$$\cos\theta=1-\frac{l}{R},$$

where

$$A^2=\frac{2R}{2R-l}(x_0^2+lx_0x_0'+lRx_0'^2/2),$$
$$B^2=\frac{2R}{2R-l}(y_0^2+ly_0y_0'+lRy_0'^2/2),$$

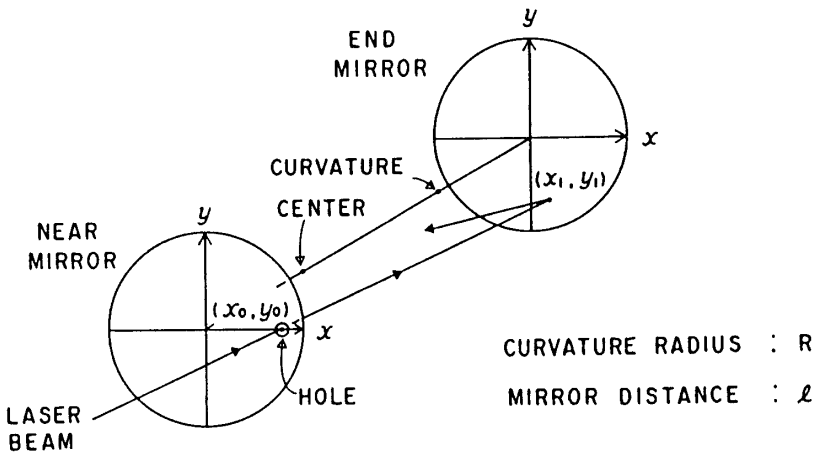

Fig. D.1 Coordinate system of the delay line with radius of curvature R and mirror distance l. The delay line axis is defined by the line crossing the curvature centers of both mirrors.

$$\tan \alpha = \frac{\sqrt{2R/l-1}}{1+Rx_0'/x_0},$$
$$\tan \beta = \frac{\sqrt{2R/l-1}}{1+Ry_0'/y_0}.$$

We can see from these equations that the beam spots on the mirror surface lie in general on an ellipse. With a proper choice of the direction of the incoming beam, the spots can be arranged in a circle, when

$$A=B,$$

and

$$\alpha=\beta\pm\frac{\pi}{2}.$$

Under this condition, the difference in polar angle between one beam spot and the next is θ; that between successive points on one particular mirror is 2θ.

The number of transits is determined by the radius of curvature of the mirrors R and their separation l. In the confocal case, when the arm length equals the radius of curvature (l=R), the total number of passes N in the delay line is four, because the difference in polar angle is exactly $\pi/2$. With a little deviation from the confocal case, we can get a large number N. If

$$2\nu\theta=2\mu\pi,$$

with μ and ν being prime to each other, then the beam returns exactly to its entrance point after N=2ν reflections in the delay line. This configuration is called re-entrance. In the re-entrance condition, the beam appears to be reflected by the back of the spherical surface of the near mirror, and the outgoing beam is to first order insensitive to tilts and lateral motions of the end mirrors.

E. Procedure of Alignment in the Vacuum

The actual procedure of alignment for bringing the two light beams to good interference in the vacuum is as follows:

(1) adjust the position and angle of the fiber-end disk so that the beam from the fiber may pass through the center of the hole in the near mirror I to the appropriate point on the end mirror I;
(2) slant the end mirror I so that the beam reflected by the end mirror I may travel to the appropriate point on the near mirror I;
(3) slant the near mirror I so that the beam reflected by the near mirror I may travel to the appropriate point on the end mirror I;
(4) adjust the arm length by translating the suspension stand of the end mirror I with the stepping motor so as to attain the desired number of reflections (N=102) with a perfect re-entrance condition;

(5) slant the beamsplitter, the end mirror II, and the near mirror II so that the same optical configuration as arm I may be realized;
(6) adjust the angle of the near mirror I and II and adjust the mirror separation in one arm so as to attain good contrast of interference;
(7) and finally improve the contrast of interference by slanting all the delay-line mirrors and, consequently, moving the beam spots on the mirrors.

The last procedure is, in principle, not necessary, if the mirrors are made with a perfect figure. Unfortunately the mirrors used are not so regular and thus the wave front of the beam after many reflections is much distorted, which results in rather a poor contrast of interference. In order to reduce the distortion of the wave front to a minimum, we can set the beam spots on the most regular parts of the mirrors. In practice we move the beam spots on the mirrors by slanting the delay-line mirrors and then search for the best configuration in terms of interference contrast.

F. RF Dark-Fringe Locking

(i) Modulation Voltage

The optimum modulation index m for the typical set-up in our interferometer is relatively high, $m \simeq 1.10$, which corresponds to a modulation voltage of 350 $V_{p\text{-}p}$ applied to the Pockels cell—its efficiency is 5.1×10^{-10} m/V. In the actual case, much smaller voltages (140 $V_{p\text{-}p}$; $m \simeq 0.44$) were used so as to prevent discharge in the vacuum, which would cause an apparent coating on the polished faces of the Pockels cell crystals and spoil it. Actually, we have suffered such discharge with higher modulation voltages (about 200 $V_{p\text{-}p}$) and spoiled Pockels cells a few times.

(ii) Modulation Frequency

The modulation frequency should be in a frequency range where the laser intensity fluctuation should be limited by shot noise of the laser light. Otherwise, the laser intensity fluctuation at the modulation frequency will be down-converted and become apparent even around 1 kHz in the interferometer output. In addition, too high a modulation frequency is difficult to handle. Therefore, a modulation frequency of around 10 MHz, which agrees to above demands, was chosen.

Since the beam passes through the Pockels cell twice, before and after the delay line, the exact modulation frequency should be set in such a manner that the modulation at the two passages adds in phase. Otherwise some cancellation of the modulation may occur, which results in decreasing the effective modulation index m. Therefore, the frequency tuning is indispensable to make the best use of the relatively low modulation voltages applied to the Pockels cell.

The method of tuning the modulation frequency to the delay line is as follows. If the beams before and after the delay line are phase modulated with the exactly opposite phase, the resultant modulation disappears perfectly. As a result, the demodulated signal will also disappear, which can indicate the worst-tuned frequency. This occurs every 300 kHz in the modulation frequency, because time delay in the delay line is 3.3 μsec. In the actual set-up, the modulation is totally cancelled at a modulation frequency of 8.795 MHz and 9.093 MHz around 9 MHz. Therefore, the modulation frequency has been tuned to 8.944 MHz which is exactly in the middle point between

two worst-tuned frequencies.

(iii) O/E Preamplifier

A fast PIN-photodiode (S1722–02, Hamamatsu Photonics) is used for detection of the interference light, because of its appropriate effective area (4.1 mm ø; 13.2mm^2).

The photodiode is combined with capacitors and coils in the first stage in such a way that the 9 MHz signal is made resonant with a bandwidth of 1 MHz and, to the contrary, the undesirable 18 MHz signal is suppressed considerably. After the filtering, the 9 MHz signal is normally amplified by a transistor and an operational amplifier.

(iv) Demodulation

A passive Double Balanced Mixer (M11, R&K) is used for multiplying the output of the O/E preamplifier by the original 9 MHz modulation signal.

Since the cable connecting the O/E preamplifier to the mixer is relatively long, the resultant phase delay should be compensated for. This is done by a common phase shifter in the original 9 MHz signal just before the mixer.

Furthermore, to operate the mixer in the ideal condition, the local oscillator signal should be of appropriate amplitude at the input of the mixer.

(v) Gain from the Path Length Change to the Demodulated Signal

It is very important to know how much signal after demodulation is produced by a change of the path length, because this value is necessary to understand the behavior of the system and especially to calculate the open loop gain of the feedback system.

The most practical and easiest way of performing it is just to measure the demodulated signal without the feedback system and with rather low light power. Although this signal must, in principle, follow the natural fluctuations of the path difference of the interferometer, the high gain of the O/E preamplifier makes the output signal saturate with normally used light power. Thus, by decreasing the light power until any saturation disappears, the gain with this low laser power can be calculated from the peak-to-peak amplitude of the naturally-fluctuating demodulated signal. Since the gain must be proportional to the available light power, the gain with the typical light power can then be calculated. The measured value was 1.5×10^9 V/m for a light power of 30 mW (Fig. F.1).

(vi) Filter Amplifier

There are two paths in the feedback loops, one is a Pockels cell path and the other is a magnet-coil path. Each path has an appropriate filter amplifier as shown in Fig. F.1.

One design feature is that the integrating part below 10 Hz in the filter amplifier for the magnet-coil path is switched on just after locking the system to a dark fringe. This integral part is necessary in order to keep the system close to the dark fringe against the long term drifts of the path length difference, Otherwise the laser intensity noise may become apparent.

(vii) Transfer Function of the Locally Controlled Pendulum

Transfer function from the input voltage of the magnet-coil system to the motion of the mirrors were measured as follows. Below 10 Hz, it was done by applying voltages to the input of the magnet-coil system and measuring the caused signal in the output of LED-P.D. sensing system for the local control. Above 10 Hz, the signal caused in the

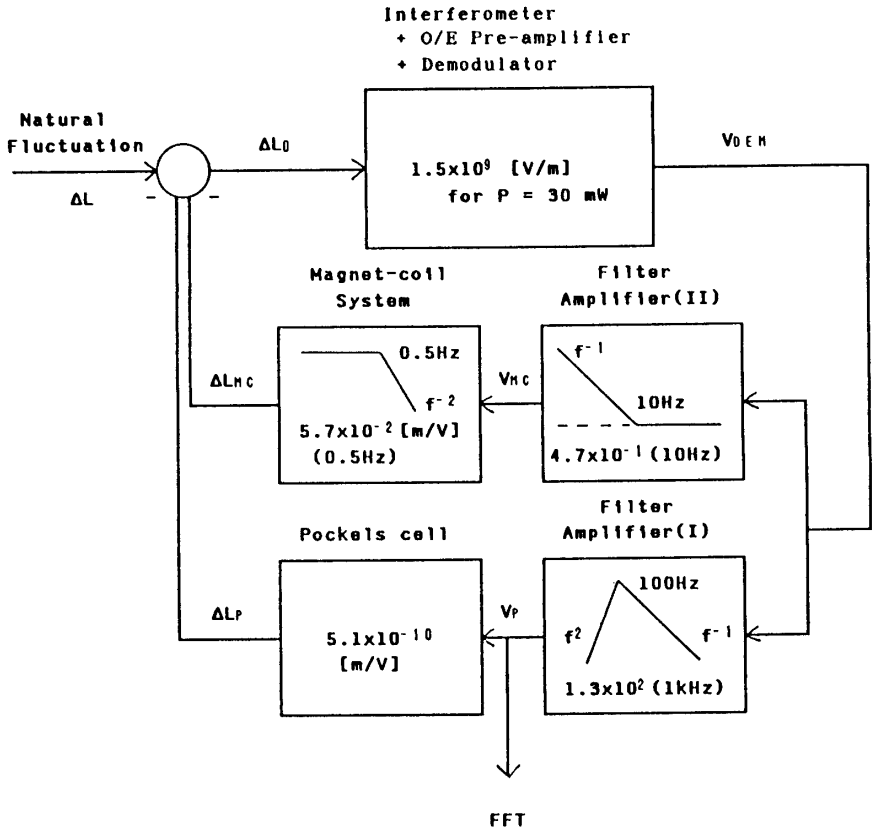

Fig. F.1 Schematic diagram of the feedback loop of the rf dark-fringe locking system. The local control is assumed to be critically damped. The integrating part below 10 Hz in the filter amplifier (II) is switched on after locking the system to a dark fringe.

output of the interferometer was measured without locking the system to the dark fringe. The measured value was approximately $5.7\times10^{-2}\times(0.5/f)^2$ m/V when the local control causes critical damping.

(viii) Stability of the System

In order to get high gain at the pendulum frequency (0.5 Hz), the slope of the open loop gain is made relatively steep below the unity gain frequency. Especially, between 0.5 Hz and 10 Hz, the slope is almost -60 dB/decade and the phase shift is close to $-270°$. The schematic diagram of the Nyquist plot of the open loop gain for the rf dark-fringe locking system is shown in Fig. F. 2. Although the contour does not enclose the point $(-1,0)$ in the figure, the feedback system is only conditionally stable; with a much lower or higher total gain, it may become unstable.

G. Linear Spectral Density

When one discusses the sensitivity of an interferometer, it is customary to express the noise in the form of linear spectral densities. In general the linear spectral density $\delta x(f)$ of a noise x(t) is defined by

$$\delta x(f)=\sqrt{2S_x(f)}\,,$$

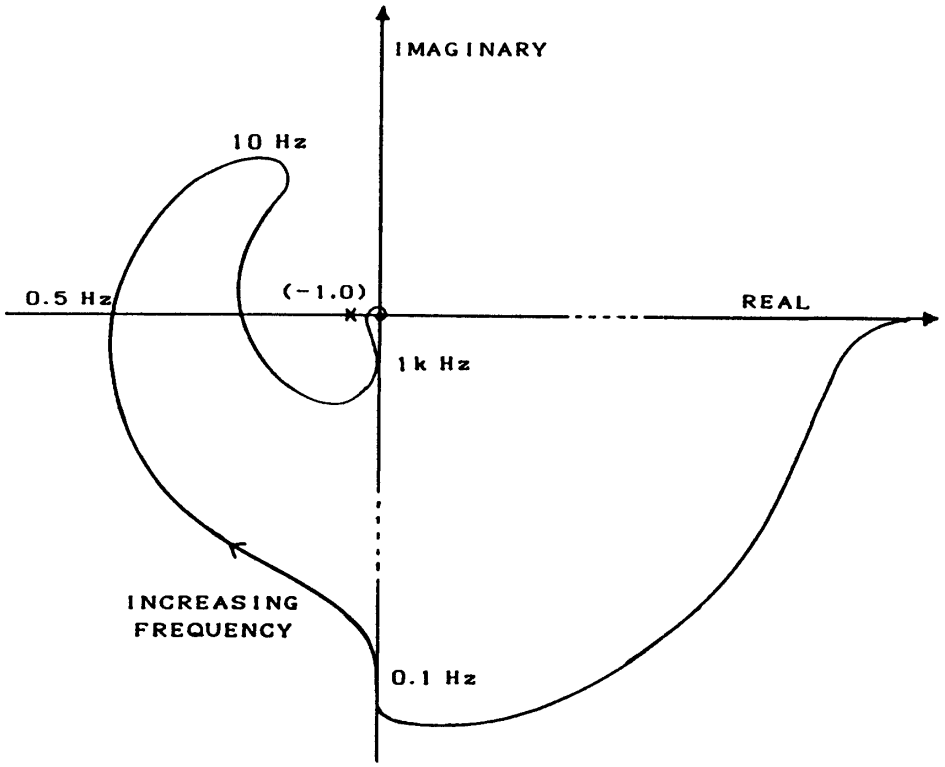

Fig. F.2 Schematic diagram of the Nyquist plot of the open loop gain for the rf dark-fringe locking system (not to scale). The feedback system is conditionally stable.

where $S_x(f)$ is the more familiar power spectral density:

$$\overline{|x(t)-\bar{x}|}^2=\int_0^\infty 2S_x(f)df.$$

where the bar indicates the average of the function.

If x(t) is the path difference between the two beams in the interferometer with the dimension of length measured in meters, then the linear spectral density δx has the dimension of $m/\sqrt{Hz}$. In the case of strain, the linear spectral density of the strain δh has the dimensions of $1/\sqrt{Hz}$.

If one observes a frequency range with a bandwidth of Δf, where the noise is supposed to be white, the rms amplitude for the strain h is given by

$$h_{rms}\simeq\delta h\ \sqrt{\Delta f}.$$

For example if an interferometer antenna has a sensitivity of $\delta h=10^{-18}/\sqrt{Hz}$ with a bandwidth of 1 kHz, the measurable strain h in this range is $3\times10^{-17}/\sqrt{Hz}$.

H. Transfer Function of the Pendulum Isolation

Instead of the actual suspension system, let's consider a single pendulum suspended by one wire to simplify the model. Assuming the wire length l, the linear mass density

of the wire γ, and the pendulum mass m, we can calculate the transfer function of the displacement from the suspension point to the mass [9], which is given by

$$H(f)=\frac{1}{\cos kl-(m/\gamma)k\sin kl},$$

where k is the propagation constant determined by the propagation velocity:

$$k=\frac{2\pi f}{v_p},$$

$$v_p=\sqrt{mg/\gamma}.$$

For $kl << 1$, the well-known pendulum-mode resonance frequency and transfer function are derived:

$$f_p=\frac{1}{2\pi}\sqrt{g/l},$$

$$H(f)=\frac{1}{1-(f/f_p)^2}.$$

In our case with a wire length of 1.12 m, the resonance frequency of the pendulum is 0.47 Hz.

The wire-mode resonance frequency can be derived as

$$f_n=n\frac{\sqrt{mg}}{2l\sqrt{\gamma}}.$$

Since our mirror is suspended by two wires, the effective mass is half of the actual mirror mass. For the values used (m=1.2 kg and $\gamma=3.2\times10^{-4}$ kg/m) the lowest resonance frequency is 61 Hz. Clearly we should use a wire with smaller γ so that the pendulum behaves like an ideal pendulum with an isolation approximately proportional to f^{-2} over a large range of frequencies before being compromised by wire resonances.

The finite Q-value of the pendulum motion may also deteriorate the ideal transfer function of the pendulum.This is the case if the damping depends on the relative velocity between the mass and its suspension point, e. g. by internal friction of the suspension wire, but not in case of damping e. g. due to the rest gas. The deteriorated transfer function shows a transition from

$$H(f)\simeq(f_p/f)^2$$

to

$$H(f)\simeq f_p/(fQ)$$

at a transition frequency of

$$f_{TR}=f_p\ Q.$$

The actual Q-value of our pendulum is approximately 800 and thus the transition frequency is at about 400 Hz. Since our typical vacuum pressure is below 10^{-3} mbar, a Q-value of 800 cannot be due to damping from the rest gas.